Journal of Medicinal Chemistry

pubs.acs.org/jmc Article

Novel Class of Colony-Stimulating Factor 1 Receptor Kinase Inhibitors Based on an *o*-Aminopyridyl Alkynyl Scaffold as Potential Treatment for Inflammatory Disorders

Zhicheng Xie,[⊥] Bing Wu,[⊥] Yingqiang Liu,[⊥] Wenming Ren, Linjiang Tong, Caigui Xiang, Aihuan Wei, Yuanzhuo Gao, Limin Zeng, Hua Xie,* Wei Tang,* and Youhong Hu*

Cite This: https://dx.doi.org/10.1021/acs.jmedchem.9b01912 Read Online

ACCESS | Metrics & More | Article Recommendations | Supporting Information

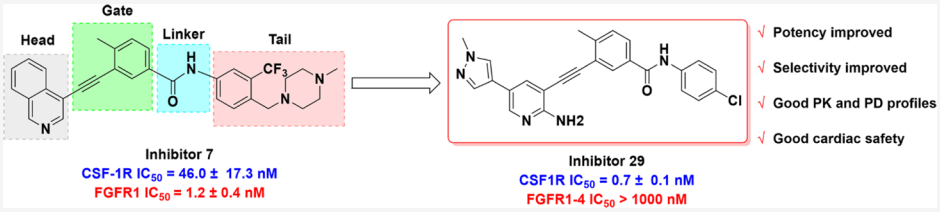

ABSTRACT: Colony-stimulating factor 1 receptor (CSF-1R) is involved in inflammatory disorders as well as in many types of cancer. Based on high-throughput screening and docking results, we performed a detailed structure−activity-relationship study, leading to the discovery of a new series of compounds with nanomolar IC_{50} values against CSF-1R without the inhibition of fibroblast growth factor receptors. One of the most promising hits, compound **29**, potently inhibited CSF-1R kinase with an IC_{50} value of 0.7 nM, while it showed no inhibition to the same family member FMS-like tyrosine kinase 3. Compound **29** displayed excellent anti-inflammatory effects against RAW264.7 macrophages indicated by significant inhibition against the activation of the CSF-1R pathway with low cytotoxicity. In addition, compound **29** exhibited strong in vivo anti-inflammatory efficacy alongside favorable drug characteristics. This novel compound **29** may serve as a new drug candidate with promising applications in inflammatory disorders.

INTRODUCTION

A macrophage colony-stimulating factor-1 receptor (CSF-1R, also known as FMS)[1] is a class III receptor tyrosine kinase family, which also includes FMS-like tyrosine kinase 3 (FLT-3), stem cell factor receptor (KIT), and platelet-derived growth factor receptor (PDGFR) α and β. CSF-1R is primarily expressed in macrophage lineages including monocytes, tissue macrophages, dendritic cells, and osteoclasts.[2] It plays an important role in signal transduction through CSF-1/CSF-1R for the differentiation, survival, proliferation, adhesion, and migration of monocyte/macrophage lineage cells.[2] However, CSF-1/CSF-1R axis overactivation through downstream pathways such as PI3K/AKT/NF-κB, PKC/NF-κB, and ROS/RAS/RAF/MAPK[3−6] may lead to aberrant expression of pro-inflammatory cytokines including tumor necrosis factor-α (TNF-α) and interleukin-6 (IL-6), among others. The augmentation of these pro-inflammatory cytokines can promote the pathogenesis of various types of cancer, bone disorders, and inflammatory diseases. Various groups have shown that CSF-1R inhibition has the potential to prevent erosions, reduce symptoms of rheumatoid arthritis (RA) and bone osteolysis,[7−9] and slow the progression of amyotrophic lateral sclerosis.[10] Moreover, recent research has demonstrated that elimination of microglia through CSF-1R inhibition could curtail plaque formation in an Alzheimer's disease in vivo model.[11] These experiments and others identify CSF-1R as a suitable target for macrophage-induced inflammatory disease. Thus, suppression of the CSF-1/CSF-1R axis through CSF-1R selective small-molecule inhibitors is of great promise in anti-inflammation therapy.

A number of small-molecule CSF-1R inhibitors have been reported to date.[12] For instance, PLX3397 (**1**),[13] an oral tyrosine kinase inhibitor of CSF-1R, KIT, and mutant FLT-3 was approved by the U.S. Food and Drug Administration (FDA) in 2019 as an orphan drug for the treatment of pigmented villonodular synovitis (PVNS or dt-GCT). In addition to PLX3397, BLZ-945 (**2**),[14] ARRY-382 (**3**),[15] JNJ-40346527 (**4**),[16] PLX7486 (**5**, structure undisclosed),[17] and DCC-3014 (**6**, structure undisclosed)[18] are currently under clinical development (Figure 1). However, most of the CSF-1R small-molecule inhibitors in development unfortunately exhibit poor kinase selectivity. In particular, it has been difficult for the

Received: November 26, 2019

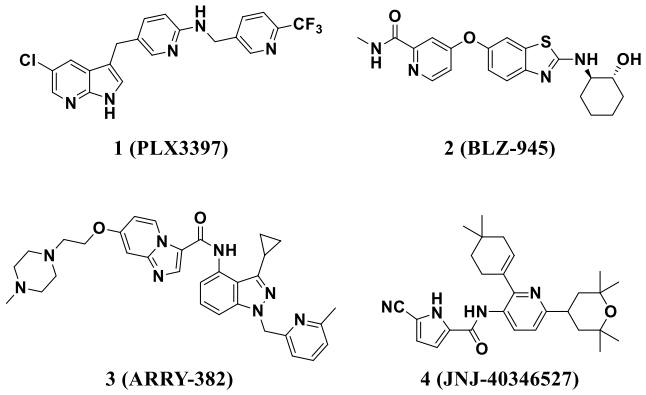

Figure 1. Representative chemical structure of CSF-1R kinase inhibitors.

field to distinguish homologous kinases such as FLT-3, KIT, PDGF-α/β, and so forth. Recent research demonstrates that the simultaneous inhibition of FLT-3 and KIT could result in profound side effects including myelosuppression and hair depigmentation.[19] Therefore, there is large demand to develop novel CSF-1R inhibitors exhibiting favorable chemical scaffolding and compound properties for inflammatory disease therapy. Herein, we report potent and selective CSF-1R inhibitors with an *o*-aminopyridylene scaffold that do not inhibit FLT-3.

Our previously developed diarylenes-based multitargeted kinase inhibitor **7**[20] exhibited potent activity against fibroblast growth factor receptors (FGFRs) and moderated inhibitory activity against CSF-1R. Removal of the *N*-methylpiperazine tail produced a novel CSF-1R inhibitor displaying excellent selectivity to CSF-1R over FGFRs. Following this identification, structure−activity relationship (SAR) studies adjusted "head", "gate", "linker", and "tail" moieties, leading to the discovery of a novel, highly potent, and selective CSF-1R kinase inhibitor without FGFR and FLT-3 inhibition, compound **29**. In addition, **29** also displayed promising pharmacokinetic (PK) properties and excellent anti-inflammatory efficacy in both in vitro assays using RAW264.7 macrophages and in vivo investigations utilizing LPS-induced mouse models of inflammation.

CHEMISTRY

Synthesis of the designed compounds **8**−**22** (Tables 1 and 2) is outlined in Scheme 1. Commercially available halogenated heteroaromatic compounds (**38**) were reacted with ethynyltrimethylsilane through Sonogashira cross-coupling reaction to give the intermediates (**39**). Compounds **41** were prepared in high yields by the condensation reaction between 4-substituted-3-halogenobenzoic acids (**40**) with the corresponding anilines. The coupling of **41** with **39** gave the final products (**8**−**15**) and intermediates (**42**). Compound **42** was subsequently used in a Suzuki reaction with the boric acid ester to produce the designed molecules (**16**−**22**). To explore the SAR of R_2 moiety (Table 3), an efficient synthetic route was designed as shown in Scheme 2. Methyl 3-iodo-4-methylbenzoate (**43**) was coupled with 5-bromo-3-((trimethylsilyl)ethynyl) pyridin-2-amine (**39i**) at room temperature to generate the intermediate, which was further coupled with the related boric acid ester to produce the key intermediate (**44**). The designed molecules (**23**−**33**) were readily prepared by hydrolysis of methyl ester (**44**) and then followed by condensation with the different substituted anilines. Compounds **34**−**37** (Table 4) were prepared as illustrated in Scheme 3. The amides **48a**−**c** were obtained by a condensation reaction with **46** and **47**. The designed linear molecule **34** and reversed amide compound **35** were obtained through a Sonogashira cross-coupling reaction and a Suzuki reaction starting from the intermediates **48a** and **48b** with **39i** and 1-methyl-4-(4,4,5,5-tetramethyl-1,3-dioxolan-2-yl)-1*H*-pyrazole, respectively. The amide bond of **48c** was further methylated or reduced to give the intermediates **49** and **50**, which is followed by two-step Pd-catalyzed cross-coupling reaction to provide the final compounds **36** and **37**.

RESULTS AND DISCUSSION

Design Rationale and SAR. Through screening of our in-house kinase inhibitor library, we identified a number of compounds that displayed CSF-1R kinase inhibition including compounds **7** and **8** (Figure 2), which exhibited moderate suppression of CSF-1R with an IC_{50} value of 46.0 ± 17.3 and 23.4 ± 8.7 nM, respectively. Interestingly, differences in molecular structure revealed that FGFR inhibition activity (compound **7**, FGFR1 IC_{50} = 1.2 ± 0.4 nM; compound **8**, FGFR1-4 IC_{50} > 1000 nM) could be eliminated through removal of a trifluoromethyl group and a *N*-methylpiperazine tail. To identify structure-dependent differential binding modalities, we conducted preliminary computational investigations (Figure 3). The docking results of **7** and **8** with FGFR1 (PDB code: 4V04) (Figure 3B,C) indicate potential binding with the inactive DFG-out conformation (represented by Phe642) of FGFR1 utilizing a type II binding mode. The trifluoromethyl group and *N*-methylpiperazine tail present in compound **7** likely form interactions crucial for FGFR1 kinase binding (e.g., multihalogen bonds with Ile546 and Ile639, a cation−π interaction with His621, electrostatic interactions with His621 and Cys619, water-bridged hydrogen bonds between the *N*-methylpiperazine motif and backbone carbonyl oxygen atom of Ile620 and His621, among others) that are not present in compound **8** because of the removal of key pharmacophores integral to FGFR binding (**8**, FGFR1-4 IC_{50} > 1000 nM). Compounds **7** and **8** were then docked into CSF-1R (Figure 3D−F) to determine the factors contributing to compound **8**'s increased CSF-1R potency poststructural modification from **7**. Although both **7** and **8** fit the DFG-out conformation of CSF-1R as represented by Phe797 (Figure 3D,F), the large *N*-methylpiperazine group present in compound **7** sterically repulsed the JM (juxtamembrane) domain (Figure 3E) while **8** recruited the JM domain and formed novel contacts (represented by a $\pi-\pi$ stacking with Trp550) with JM residues upon binding to CSF-1R (Figure 3F). Consistent with prior research, unlike compound **7** which acts as a conventional type II inhibitor, **8** binds to an autoinhibited CSF-1R and engages the JM region on a more physiologically common full-length CSF-1R protein state, leading to increased potency and reduced secondary kinase cross-reactivity.[13] As a novel-type II inhibitor, **8** exhibited excellent selectivity to CSF-1R over FGFRs (CSF-1R IC_{50} = 23.4 ± 8.7 nM; FGFR1-4 IC_{50} > 1000 nM). Consequently, compound **8** was chosen as a lead compound for further SAR study.

Based on the type II kinase inhibitor-binding element hybrid design strategy,[21] we initiated the SAR investigation by varying the "head", "gate", "linker", and "tail" moieties. First, as a hinge-binding element, the isoquinoline introduced low atomic

https://dx.doi.org/10.1021/acs.jmedchem.9b01912
J. Med. Chem. XXXX, XXX, XXX−XXX

Table 1. SAR Exploration Focused on the Het. Moiety[a]

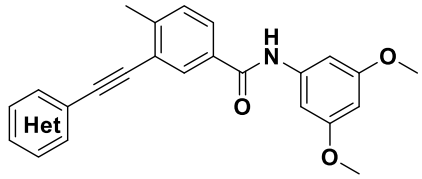

Compd.	Het.	CSF-1R (IC_{50}, nM)
8	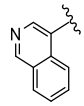	23.4 ± 8.7
9	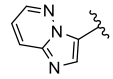	25.1 ± 8.0
10	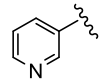	218.9 ± 153.4
11	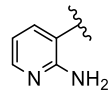	28.5 ± 9.3
12	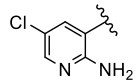	16.6 ± 5.0
13	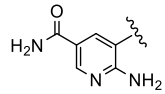	3.5 ± 1.3
14	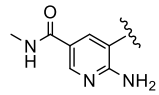	8.1 ± 1.6
15	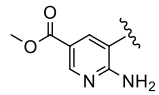	5.5 ± 1.2
16	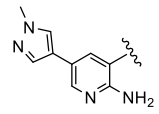	2.6 ± 0.4
PLX3397	-	15.8 ± 9.3

[a]All IC_{50} values (mean ± SD) against CSF-1R kinase were obtained from inhibition ratios at different concentrations (0.1−1000 nM) from two independent experiments performed in duplicate.

economic efficiency and unfavorable drug characteristics because of its large rigid planar conjugated system. Therefore, we first explored the effect of "head" (Het.) moiety and synthesized a series of compounds with varying aromatic heterocycles (Het). The biochemical potency of newly synthesized compounds against CSF-1R was measured and is displayed in Table 1. The isoquinoline in **8** was replaced with the dominant fragment imidazo[1,2-*b*]pyridazine in Ponatinib and a ring-opening pyridine, leading to compound **9** and monocyclic compound **10**, respectively. However, compound **10** lost more than 9-fold activity against CSF-1R in comparison with **8**. The binding modes of PLX3397 (Figure 3A) and **8** (Figure 3C) suggest that the introduction of an amino group can serve as a hydrogen bond donor and form an extra hydrogen bond with a Glu664 backbone carbonyl in the hinge domain, as in the binding mode of PLX3397. The instillation of a $-NH_2$ group in the ortho-position of a pyridine N atom (**11**, IC_{50} = 28.5 ± 9.3 nM) could thus significantly increase

https://dx.doi.org/10.1021/acs.jmedchem.9b01912
J. Med. Chem. XXXX, XXX, XXX−XXX

Table 2. SAR Exploration Focused on the Substitution (R_1) Moiety[a]

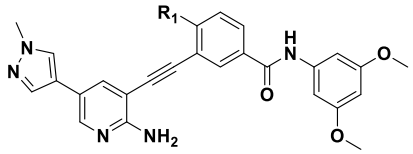

compd.	R_1	CSF-1R (IC_{50}, nM)
16	$-CH_3$	2.6 ± 0.4
17	−H	16.1 ± 1.9
18	$-CH(CH_3)_2$	>1000
19	$-OCH_3$	263.0 ± 59.3
20	−F	160.3 ± 22.7
21	−Cl	6.5 ± 2.1
22	$-CF_3$	>1000
PLX3397		14.0 ± 2.9

[a]All IC_{50} values (mean ± SD) against CSF-1R kinase were obtained from inhibition ratios at different concentrations (0.1−1000 nM) from two independent experiments performed in duplicate.

Table 3. SAR Exploration Focused on the Substitution (R_2) Moiety[a]

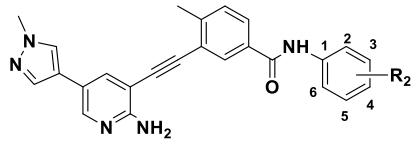

compd.	R_2	CSF-1R (IC_{50}, nM)
16	3,5-$(OCH_3)_2$	2.6 ± 0.4
23	−H	6.5 ± 1.7
24	2-OCH_3	20.2 ± 4.6
25	3-OCH_3	1.4 ± 0.1
26	4-OCH_3	1.4 ± 0.2
27	2-Cl	318.0 ± 54.2
28	3-Cl	1.3 ± 0.3
29	4-Cl	0.7 ± 0.1
30	3-CF_3	2.4 ± 0.5
31	4-CF_3	3.0 ± 0.5
32	2,4-$(Cl)_2$	5.9 ± 0.1
33	3,4-$(Cl)_2$	10.8 ± 0.6
PLX3397		17.3 ± 1.2

[a]All IC_{50} values (mean ± SD) against CSF-1R kinase were obtained from inhibition ratios at different concentrations (0.1−1000 nM) from two independent experiments performed in duplicate.

potency to that of compound **8**. Structural differences between compound **8**, **11**, and PLX3397 revealed an extra binding pocket in the 5-position outwardly extending from the *o*-aminopyridine ring. With this in mind, we hybridized compound **11** and PLX3397 to create compound **12**, which yielded improvements in activity. Docking studies to CSF-1R identified plausible binding modes of compound **12** (Figure 4A): "head" *o*-aminopyridine forms double hydrogen bonds with the hinge regions that are integral to high potency. The middle benzene ring passes through the "gate" area and allows the molecule to fit in a hydrophobic pocket. As a "linker", the amide motif then forms critical hydrogen bonds with the conserved DFG-motif (Asp796, Phe797, Gly798) and Glu633 in the c-helix of CSF-1R. Finally, the "tail" of compound **12** (a benzene ring) binds to the receptor through establishing a $\pi-\pi$ stacking interaction with a Trp550 residue in the JM domain. Subsequently, we discuss the detailed SAR based on compound **12** binding modalities.

A series of compounds with different substituent groups to replace the 5-chloro of Het. in compound **12** were synthesized to understand the importance of this substituent in the "head" (Table 1). As shown in the binding mode of **12** (Figure 4A), the substituent at the 5-position of *o*-aminopyridine ring was bound in a relatively large hydrophilic pocket, and the introduction of polar groups with heteroatoms or heterocycle could increase potency because of the electronic fit or the extra $\pi-\pi$ stacking with Tyr665. Interestingly, changing the Cl atom to a carbonyl group (**13**−**15**) remarkably increased the potency against CSF-1R. Further increasing the size and polarity of the substituent with a *N*-methylpyrazolyl group (**16**) resulted in the increasing potency of compound **16** for the inhibition of CSF-1R with an IC_{50} value of 2.6 ± 0.4 nM. Based on the results discussed above, the SAR on "head" (Het.) moiety indicates binding in a suitable hydrophilic pocket of CSF-1R that is closed to the solvent-exposed areas.

Scheme 1. Synthesis of Compounds 8−22[a]

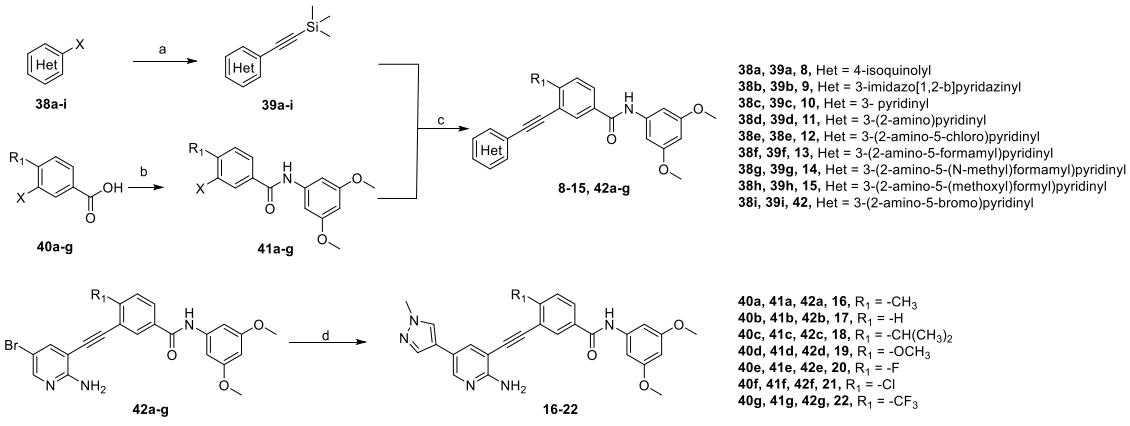

[a]Reagent and conditions: (a) X = Br: trimethylsilylacetylene, $Pd(PPh_3)_2Cl_2$, CuI, MeCN/Et_3N (4:1, v/v), 80 °C, 4 h; X = I: ethynyltrimethylsilane, $Pd(PPh_3)_2Cl_2$, CuI, Et_3N, rt, 6 h; (b) HATU, DIPEA, DMF, rt, 4 h; (c) X = Br: $Pd(PPh_3)_2Cl_2$, CuI, CsF, Et_3N, MeCN, 80 °C, 4 h; X = I: $Pd(PPh_3)_2Cl_2$, CuI, CsF, Et_3N, MeCN, rt, 4 h; (d) 1-methyl-4-(4,4,5,5-tetramethyl-1,3-dioxolan-2-yl)-1*H*-pyrazole, $Pd(PPh_3)_4$, K_2CO_3, toulene/EtOH/H_2O (2/1/1, v/v/v), microwave irradiation, 100 °C, 20 min.

https://dx.doi.org/10.1021/acs.jmedchem.9b01912
J. Med. Chem. XXXX, XXX, XXX−XXX

Scheme 2. Synthesis of Compounds 23−33[a]

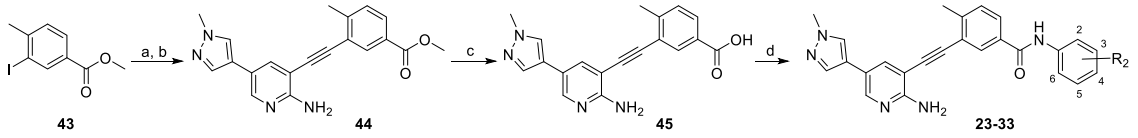

[a]Reagent and conditions: (a) **39i**, $Pd(PPh_3)_2Cl_2$, CuI, CsF, Et_3N, MeCN, rt, 5 h; (b) 1-methyl-4-(4,4,5,5-tetramethyl-1,3-dioxolan-2-yl)-1*H*-pyrazole, $Pd(OAc)_2$, X-phos, K_2CO_3, THF/H_2O (4/1, v/v), 90 °C, 6 h; (c) $LiOH{\cdot}H_2O$, $THF/MeOH/H_2O$ (4/1/1, v/v/v), rt, 12 h; (d) the substituted phenylamines, HATU, DIPEA, DMF, rt, 4 h.

Table 4. SAR Exploration Focused on the Linker Moiety[a]

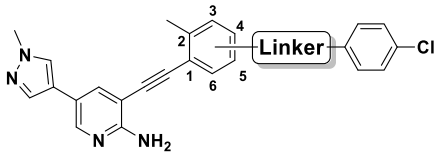

compd.	linker	CSF-1R (IC_{50}, nM)
29	5-CONH−	0.7 ± 0.1
34	4-CONH−	>1000
35	5-NHCO−	7.2 ± 1.8
36	5-CON(CH_3)−	>1000
37	5-CH_2NH−	>1000
PLX3397		12.0 ± 1.4

[a]All IC_{50} values (mean ± SD) against CSF-1R kinase were obtained from inhibition ratios at different concentrations (0.1−1000 nM) from two independent experiments performed in duplicate.

Moreover, the molecular docking results of compound **16** displayed that the *N*-methylpyrazolyl group increased its receptor binding affinity because of the extra $\pi-\pi$ stacking interactions forming between its arene π-system with the benzene ring of Try665 and a π−anion interaction with the carboxyl negative charge center of Asp670 (Figure 4B).

Because **16** exhibited potent inhibitory efficacy against CSF-1R, we maintained the "head" moiety with 5-*N*-methylpyrazolyl-2-aminopyridine and further explored the "Gate" (R_1) moiety (Table 2). Compound **17** to **22** were initially synthesized to elucidate the steric and electronic effects present at this position. It was found that methyl group replacement with hydrogen (**17**) and isopropyl (**18**) decreased potency, with dramatic loss in activity upon isopropyl introduction. This finding indicates that optimal R_1 group sizing is crucial for potency. Subsequently, substituent variations at this position with differing electronic effects (MeO in **19**, F in **20**, and CF_3 in **22**) substantially decreased activity. A Cl group addition (compound **21**) yielded similar potencies to compound **16**. These results indicate that the R_1 substituent binds in a specific hydrophobic binding pocket with steric and electronic requirements. The importance of this methyl in maintaining high potency against the CSF-1R kinase was found by docking compound **16** into CSF-1R, as shown in Figure 5. The methyl group of **16** was bound in a specifically sized hydrophobic pocket formed by Val596, Ala614, Lys616 and the gatekeeper Thr663 via extensive van der Waals forces, and hydrophobic interactions with the receptor. More importantly, computational analysis hypothesized approximate orthogonal conformations between the two aromatic systems of **16** fixed by this methyl group, which aided CSF-1R binding (Figure 5). Given the outstanding potency of inhibitor **16**, the R_1 moiety (methyl group) was further fixed in the follow SAR investigation.

Computational studies suggest that the substituted benzene ring "tail" stabilizes the auto-inhibited CSF-1R state by forming interactions directly with the JM domain (represented by a $\pi-\pi$ stacking interaction with JM-Trp550), which is crucial for potency and selectivity improvement. To maintain this key interaction, differential substituent effects were introduced into the aniline ring (Table 3). 3,5-Dimethoxyl groups were first removed to yield compound **23**, which also exhibited potency to CSF-1R. Then, we investigated the potential impact of phenyl ring substituents by introducing electronic effects (MeO, Cl, CF_3) at the 2-, 3-, and 4- positions of the benzene ring (**24**−**31**). Ortho-substitution with electron-donating group MeO yielded lowered activity as compared to **23**, whereas the meta- and para-substitution patterns of methoxyl groups (**25** and **26**) improved potency against CSF-1R. A similar phenomenon was observed with the substitution patterns of Cl (**27**−**29**). These findings suggest that the 3- or 4- positions might optimally suppress the kinase function of CSF-1R, with the 4-chloro substitution (**29**) exhibiting the highest potency (IC_{50} = 0.7 nM). In addition, CF_3 substitution at the 3- or 4- position maintained CSF-1R potency. Further investigating di-substitutional effects at favorable meta- and

Scheme 3. Synthesis of Compounds 34−37[a]

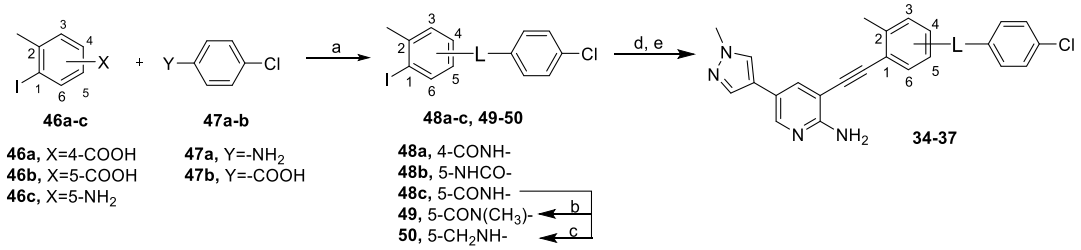

[a]Reagent and conditions: (a) HATU, DIPEA, DMF, rt, 4 h; (b) MeI, NaH, THF, 0 °C to rt, 5 h; (c) $BF_3{\cdot}THF$ (1 M), THF, rt, 12 h; (d) **39i**, $Pd(PPh_3)_2Cl_2$, CuI, CsF, Et_3N, MeCN, rt, 4 h; (e) 1-methyl-4-(4,4,5,5-tetramethyl-1,3-dioxolan-2-yl)-1*H*-pyrazole, $Pd(PPh_3)_4$, K_2CO_3, THF/EtOH/H_2O (2/1/1, v/v/v), microwave irradiation, 100 °C, 20 min.

https://dx.doi.org/10.1021/acs.jmedchem.9b01912
J. Med. Chem. XXXX, XXX, XXX−XXX

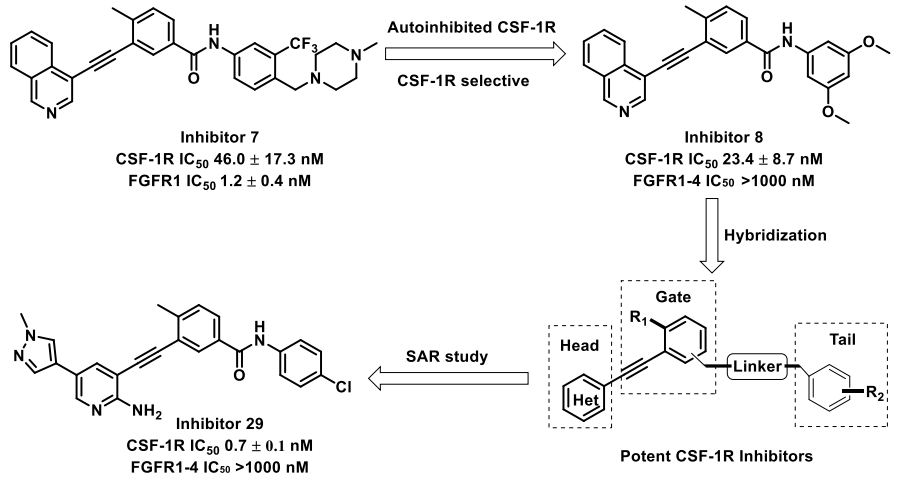

Figure 2. Development schematic of novel *o*-aminopyridylene scaffold-based CSF-1R selective inhibitor **29** by structural modification of the previously designed FGFR inhibitor **7**.

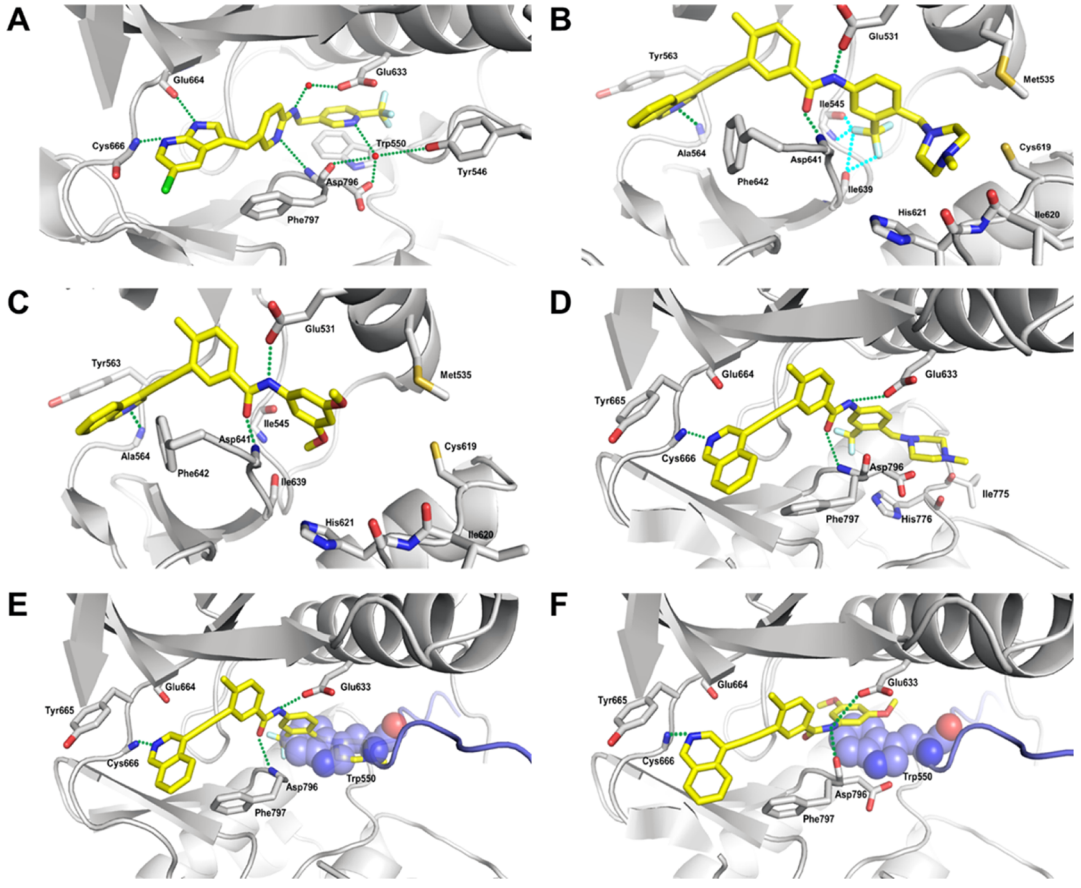

Figure 3. Binding mode analysis of compounds **7** and **8** to FGFR and CSF-1R kinases. (A) Crystal structure of CSF-1R kinase domain with PLX3397 (PDB code 4R7H). (B) Molecular docking of compound **7** into FGFR1 kinase (generated from PDB code 4V04). (C) Molecular docking of compound **8** into FGFR1 kinase (generated from PDB code 4V04). (D) Molecular docking of compound **7** into CSF-1R kinase (generated from PDB code 4R7I). (E) Structure illustration of compound **7** displaces the JM domain of CSF-1R kinase (generated from PDB code 4R7H and 4R7I). (F) Structure illustration of compound **8** recruits the JM domain of CSF-1R kinase (generated from PDB code 4R7H).

para-positions (**33**) did not display synergistic effects. These findings indicate that benzene ring electron density plays a minor role in potency, whereas benzene ring spatial orientation to JM-Trp550 contributes greatly to activity through $\pi-\pi$ interactions, which requires suitable orientations between the benzene and indole rings of JM-Trp550. The steric hindrance of ortho-substituent groups may disrupt the optimal orientation between the two aromatic rings to lead the potency loss. Thus, the mono-substitution at meta- or para-position is more favorable, especially the *para*-chloro substitution (**29**) is optimal.

Finally, we explored the "linker" moiety by fixing the "head", "gate", and "tail" as shown in Table 4. Changing the amide from the 5-position to the 4-position to yield a linear molecule

https://dx.doi.org/10.1021/acs.jmedchem.9b01912
J. Med. Chem. XXXX, XXX, XXX−XXX

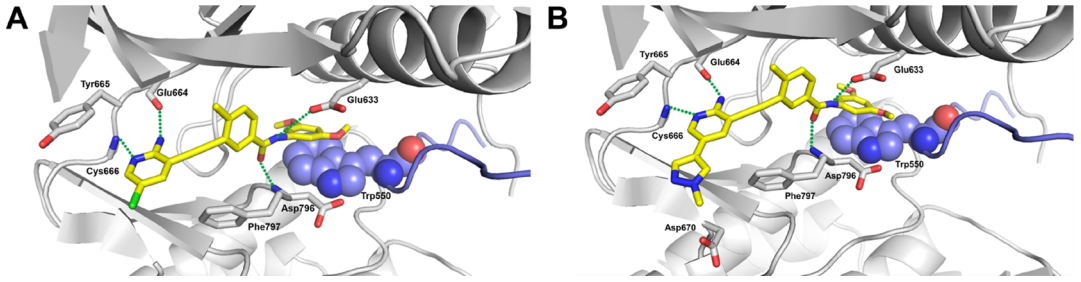

Figure 4. Schematic illustration of the SAR exploration rationale. (A) Binding mode study of compound **12** in CSF-1R kinase (generated from PDB code 4R7H); (B) binding mode study of compound **16** in CSF-1R kinase (generated from PDB code 4R7H).

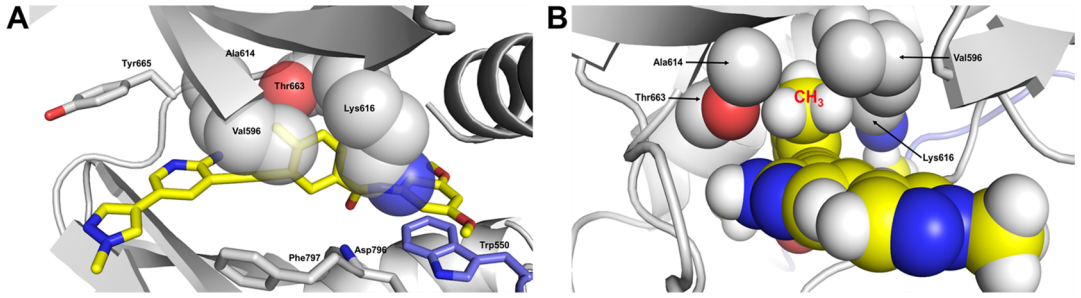

Figure 5. Molecular modeling analysis of the binding mode of compound **16** in CSF-1R kinase. (A) Binding mode study of **16** in CSF-1R kinase (generated from PDB code 4R7H); (B) Approximate orthogonal conformation of the diarylethyne system was controlled by the methyl group in the middle benzene ring.

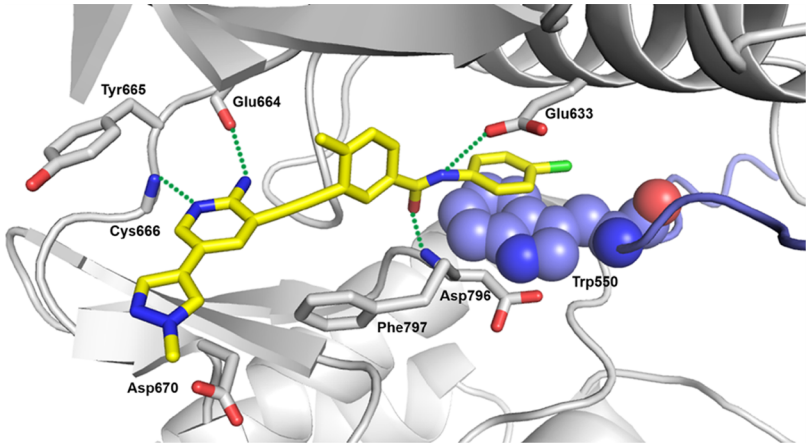

Figure 6. Binding mode study of inhibitor **29** in CSF1R kinase (generated from PDB code: 4R7H).

(**34**) resulted in total loss of inhibitory potency because of its high rigidity and steric resistance upon binding to the target protein. Furthermore, a reversed amide counterpart of the linker in **29** (**35**) resulted in decreasing activity to CSF-1R. Amide blockage by methylation of −NH (**36**) and carbonyl saturation (**37**) also led to total loss of potency. These results indicate that the 5-amine linker is crucial for CSF-1R activity because of the key hydrogen bonding established between the amide −NH and carbonyl moieties with the DFG-motif and Glu633 in the c-helix of CSF-1R.

To better understand the interaction between the synthesized compounds and CSF-1R kinase, molecular docking of the highest potent compound **29** into the ATP binding site of CSF-1R kinase (PDB code: 4R7H) was performed. The binding model is depicted in Figure 6. Serving as a desirable hinge binding element, the 5-(*N*-methyl)pyrazol-2-amino pyridine formed double hydrogen bonds with the hinge region (the nitrogen of pyridine with amino hydrogen atom of Cys666 and 2-amino hydrogen of pyridine with the carbonyl oxygen atom of Glu664). Beyond this, the aromatic system formed a $\pi-\pi$ stacking interaction with the benzene ring of Tyr665 and the *N*-methyl pyrazol, which could enhance the binding affinity through a $\pi-$anion interaction with the negatively charged carboxyl center of Asp670. Thus, this "head" motif likely plays a key role in CSF-1R interactions. The alkynyl linker connects the hinge-binding element with the back-pocket moiety because of its favorable overall orientation, while the middle phenyl ring of **29** binds in a hydrophobic pocket to form a $\pi-$cation interaction with the positively charged center of Lys616. Furthermore, the methyl group of the phenyl ring extended to another relatively small hydrophobic sub-pocket, which may have optimized molecular conformations, resulting in the observed increased inhibitory activity against CSF-1R. The amide linker, which can form two typical hydrogen bonds with Asp796 in the DFG motif and Glu633 in the c-helix, was critical for the binding. Therefore,

https://dx.doi.org/10.1021/acs.jmedchem.9b01912
J. Med. Chem. XXXX, XXX, XXX−XXX

Table 5. Selectivity Profiling of Compound 29

	% inhibition ratio @ conc.				% inhibition ratio @ conc.		
kinases	1000 nM	100 nM	10 nM	kinases	1000 nM	100 nM	10 nM
VEGFR1	89.80	78.50	36.20	ErbB2	9.50	8.80	N.T.[a]
VEGFR2	95.50	83.60	23.20	ErbB4	1.60	6.60	N.T.[a]
VEGFR3	100.00	69.40	27.30	IGF1R	0.00	0.00	N.T.[a]
PDGFR-α	92.60	83.90	54.60	IR	0.00	2.10	N.T.[a]
PDGFR-β	87.90	70.50	14.70	FGFR1	0.00	0.00	N.T.[a]
RET	96.60	77.60	42.70	FGFR2	20.70	16.20	N.T.[a]
c-Kit	98.20	100.00	70.40	FGFR3	2.30	0.00	N.T.[a]
Flt-3	5.90	0.00	N.T.[a]	FGFR4	7.40	0.00	N.T.[a]
EGFR	0.00	7.40	N.T.[a]	BTK	8.00	0.00	N.T.[a]
Src	72.80	61.70	1.50	FAK	10.80	14.70	N.T.[a]
Abl	98.30	82.10	0.00	ITK	7.40	4.20	N.T.[a]
EphA2	92.30	31.40	N.T.[a]	ACK1	30.90	10.30	N.T.[a]

[a]N.T. = not test.

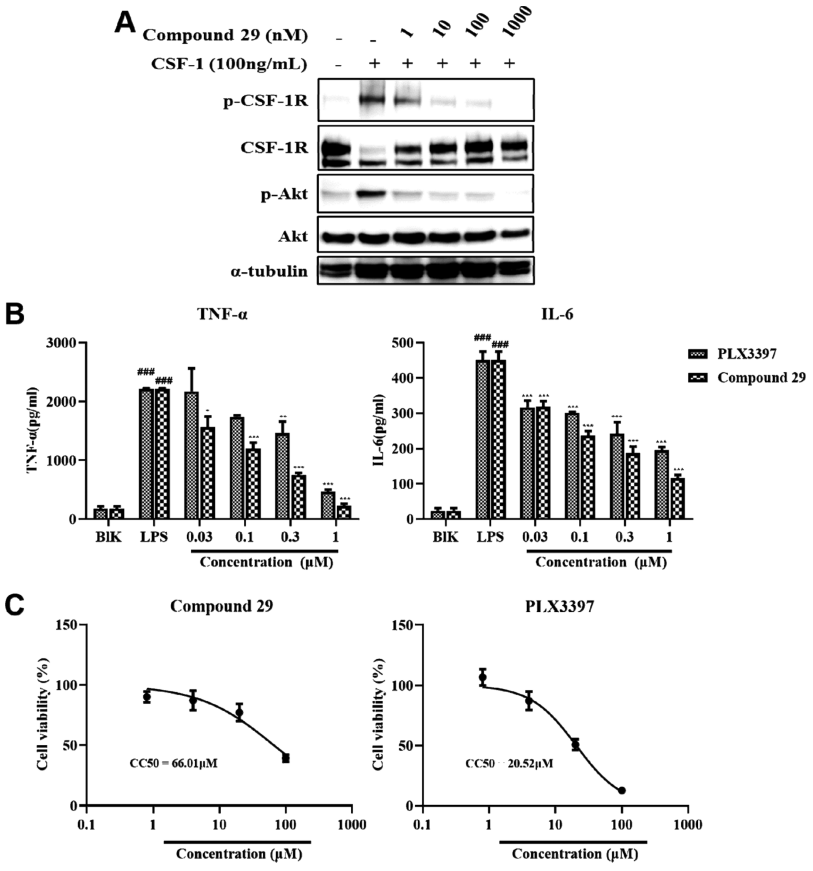

Figure 7. Cellular effects of compound **29** in the RAW264.7 cell line. (A) Compound **29** inhibited phosphorylation of CSF-1R and its downstream signaling pathway in RAW264.7 cells as determined by Western blot analysis. (B) Compound **29** exhibited potent activity on LPS-induced TNF-α and IL-6 release in RAW264.7 cells. Blk: Blank. Data are given as the mean ± standard error of the mean (SEM). Statistical analysis is performed by one-way analysis of variance (ANOVA). *P < 0.05, **P < 0.01, and ***P < 0.001 compared to LPS. #P < 0.05, ##P < 0.01, and ###P < 0.001 compared to Blk. (C) Cytotoxicity of compound **29** (CC_{50} = 66.01 μM) and PLX3397 (CC_{50} = 20.52 μM) over RAW264.7 macrophages was determined by Cell Counting Kit-8 (CCK-8).

the modification (as shown in Table 4) of this amide linker could destroy the forming of these crucial hydrogen bonds, leading to the significant loss of activity. Furthermore, we identified a $\pi-\pi$ stacking interaction between the terminal phenyl ring with a Trp550 residue in the JM domain of suitable conformation, which required a suitable spatial conformation of these two aromatic rings. Because of the steric effect, the ortho-substituent groups (represented by **24** and **27**) are unfavorable for this spatial requirement, whereas, the *para*-chloro substitution (**29**) was optimal and exhibited the highest potency.

Selectivity Profiling of Compound 29. The inhibitory activities of **29** against the other protein kinases, especially the other members of the class III growth factor receptor family, that is, FLT-3, KIT, PDGF-α and β, were also evaluated utilizing our in-house kinase assays (Table 5). The results

https://dx.doi.org/10.1021/acs.jmedchem.9b01912
J. Med. Chem. XXXX, XXX, XXX−XXX

Table 6. PK Profile of Compound 29 in Rats[a]

	$t_{1/2}$ (h)	T_{max} (h)	C_{max} (ng/mL)	AUC_{0-t} (h·ng/mL)	CL_{obs} (mL/min/kg)	MRT_{INF_obs} (h)	V_{ss_obs} (L/kg)	F (%)
p.o.								
5 mg/Kg	2.21	4.00	165.60	634.02		5.42		34.80
i.v.								
2 mg/Kg	3.33			728.93	45.98	2.30	6.34	

[a]Determined using LC/MS/MS. AUC_{0-t}: the area under the concentration time curve; MRT: mean residence time; $t_{1/2}$: elimination half-life; T_{max}: the peak time; C_{max}: the peak concentration; CL: clearance; V_{ss}: steady-state distribution volume; F: absolute bioavailability.

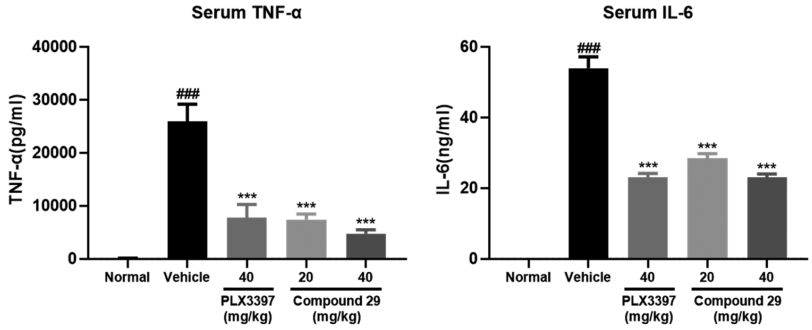

Figure 8. Inflammation cytokine concentrations in serum of the LPS-induced mice model. The mice were orally administrated with PLX3397 (40 mg/kg), compound **29** (20 and 40 mg/kg) at 4 h before intraperitoneal injection with LPS (n = 6, female). The concentration of cytokines in serum was detected at 1.5 h for TNF-α and 3 h for IL-6 by ELISA assay. Data are given as mean ± SEM. Statistical analysis is performed by one-way analysis of variance (ANOVA). *P < 0.05, **P < 0.01, and ***P < 0.001 compared to vehicle. #P < 0.05, ##P < 0.01, and ###P < 0.001 compared to normal.

showed that **29** potently inhibited the activity of KIT (inhibition rate = 70.4% at 10 nM) and PDGFR-α (inhibition rate = 54.6% at 10 nM). This result is not surprising, considering that KIT and PDGFRα/β kinases belong to the class III receptor tyrosine kinase family with highly conserved ATP binding pockets. Interestingly, **29** exhibited no inhibition against FLT-3, FGFR1-4, EGFR, ErbB2/4, and so forth. kinases at 1 μM concentration, which could greatly reduce the potential toxic effects induced by the simultaneous inhibition of FLT-3 and KIT as previously mentioned.

Cellular Evaluation of Compound 29. In light of its strong potency and reasonable target selectivity, **29** was selected as a representative molecule for further cellular evaluation. We first investigated the CSF-1R-mediated signaling pathway suppression by compound **29** in RAW264.7 cells, which harbors high kinase levels (Figure 7A). We found dose-dependent inhibition of CSF-1R and the downstream mediator, Akt, in the presence of compound **29** with significant inhibition starting at 10 nM.

CSF-1/CSF-1R signaling-mediated elevated expression of TNF-α, IL-6, and other proinflammatory cytokines contributes greatly to the pathogenesis in inflammatory diseases. Signaling interruptions with CSF-1R inhibitors have shown therapeutic effects in several inflammatory disorders by reducing the expression of TNF-α, IL-6, and other proinflammatory cytokines. Therefore, the potential anti-inflammation effects of compound **29** were investigated by measuring its capacity to suppress the release of TNF-α and IL-6 in macrophages (Figure 7B). Compound **29** suppressed TNF-α (IC_{50} = 110 nM) and IL-6 (IC_{50} = 130 nM) production in RAW264.7 macrophages with low toxicity (CC_{50} = 66.01 μM, Figure 7C), which is a stark improvement to that of PLX3397 (CC_{50} = 20.52 μM; TNF-α IC_{50} = 400 nM; IL-6 IC_{50} = 430 nM), indicating excellent anti-inflammatory effects in vitro.

In Vivo PK Evaluation of Compound 29. The preliminary in vivo PK properties of **29** were investigated in Sprague-Dawley (SD) rats, following intravenous (i.v.) and oral (p.o.) administration (Table 6). The results demonstrated that **29** exhibited favorable drug characteristics with acceptable bioavailability (F = 34.8%), moderate half-life ($t_{1/2}$ = 2.21 h), and drug exposure (AUC_{0-t} = 634.02 h·ng/mL) using 5 mg/kg oral administration. These PK properties indicate that **29** is suitable for oral administration. In addition, the blockade effect of **29** on the hERG channel was evaluated using the Qpatch Automatic Patch-Clamp assays; compound **29** exhibited low hERG-potassium-ion-channel inhibition with an IC_{50} value of >40 μM (Figure S1).

We finally evaluated the in vivo anti-inflammation efficacy of **29** in LPS-induced mouse models of inflammation (Figure 8). LPS injection in mice resulted in elevation of inflammatory cytokines, including TNF-α and IL-6, which peak at 1.5 and 3 h postinjection, respectively.[22] The compound **29** was orally administered 4 h prior to LPS injection. Treatment with compound **29** prominently reduced serum TNF-α and IL-6 concentration as compared with vehicle controls. Therefore, the results indicate that CSF-1R inhibition by compound **29** can effectively attenuate inflammation and has the potential to treat inflammatory diseases.

CONCLUSIONS

In summary, we started SAR exploration of a novel type II kinase inhibitor **8**, which identified novel *o*-aminopyridyl alkynyl scaffold-based CSF-1R selective inhibitors targeting the autoinhibited-state CSF-1R kinase without FGFR inhibition. Based on the inhibitor-binding element hybrid design strategy, we initiated the detailed SAR investigation by varying the "head", "gate", "linker", and "tail" moieties, leading to the discovery of a series of potent CSF-1R inhibitors. The instillation of a $-NH_2$ group in the ortho-position of a pyridine (head) of this scaffold forms an extra hydrogen bond with a Glu664 backbone carbonyl in the hinge domain of CSF-

https://dx.doi.org/10.1021/acs.jmedchem.9b01912
J. Med. Chem. XXXX, XXX, XXX−XXX

1R and can increase potency against CSF-1R significantly. One of the most promising compounds **29** had the highest kinase inhibitor potency against CSF-1R (IC_{50} = 0.7 ± 0.1 nM). Further kinome-screen data revealed that **29** displayed a good relative selectivity profile, which is the loss of FLT-3 potency. The effects of **29** on LPS-stimulated RAW-264.7 macrophage cells were evaluated in vitro, which exhibited low cellular toxicity and potent inhibition of the CSF-1R-mediated signaling pathways, resulting a significant suppression of the release of the inflammatory cytokines. In addition, compound **29** displayed acceptable PK properties in rats without the inhibition of hERG. Furthermore, compound **29** potent in vivo anti-inflammatory effects make it a promising candidate as potential treatment for inflammatory disorders. Further preclinical evaluation of compound **29** is currently being conducting.

EXPERIMENTAL SECTION

General Methods for Chemistry. Unless otherwise noted, all reagents and solvents employed were purchased commercially and used as received. All reactions involving air- or moisture-sensitive reagents were performed under a nitrogen (N_2) atmosphere. All reactions were conducted in microwave vials or flasks containing a Teflon-coated magnetic stirrer. Microwave irradiation experiments were performed in a CEM-Discover Lab-Mate mono-mode microwave apparatus equipped with an Intelli-VentTM pressure control system and a vertically focused IR temperature sensor. Reactions were monitored by thin-layer chromatography (TLC) on precoated TLC glass plates (silica gel GF254, 0.2 ± 0.03 mm thickness). TLC glass plates were developed in a covered chamber and were visualized with ultraviolet light using a 254 nm fluorescent indicator. Flash column chromatography was carried out on silica gel (200−300 mesh). All NMR spectra were recorded on a Bruker 400 (^{1}H: 400 MHz, ^{13}C NMR: 101 MHz, ^{19}F: 376 MHz), Bruker 500 (^{1}H: 500 MHz, ^{13}C NMR: 126 MHz, ^{19}F: 471 MHz), or Bruker 600 (^{1}H: 500 MHz, ^{13}C NMR: 151 MHz) spectrometer and referenced to the deuterium solvent (chloroform-*d*, MeOH-d_4 or DMSO-d_6). Chemical shifts (δ) were expressed in parts per million (ppm) relative to an internal standard (TMS), and coupling constants were given in Hz. Data for NMR spectra were reported as follows: chemical shift (δ ppm), multiplicity (s = singlet, br s = broad singlet, d = doublet, t = triplet, q = quartet, dd = doublet of doublets, m = multiplet), coupling constant (Hz), and integration. Low-resolution mass spectral data were measured on an Agilent 1200 series LC−MS spectrometer, and high-resolution mass spectral (HRMS) data were measured on Micromass Ultra Q-Tof. The purity of all final compounds (>95%) was determined on an Agilent 1200 series LC system (Agilent ChemStation Rev.B.03.01; column, ZORBAX Eclipse XD B-C18, 4.6 mm × 150 mm, 5 μm; flow rate, 1.0 mL/min; UV wavelength, maximal absorbance at 254 nm; temperature, ambient; and injection volume, 5 μL; mobile phase, solvent A: H_2O (with 0.1% HCOOH) and solvent B: MeOH). The gradient elution for compounds **7**−**11**, **13**−**16**, **18**−**25**, **27**−**32**, and **35**−**37**: 0−5 min, B: 50−50%; 5−10 min, B: 50−75%; 10−18 min, B: 75−75%; 18−19 min, B: 75−95%; 19−22 min, B: 95−95%; 22−23 min, B: 95−50%; 23−25 min, B: 50−50%; for compounds **12**, **17**, **26** and **33**−**34**: 0−20 min, MeOH/H_2O (0.1% HCOOH) (75/25, v/v) (see Table S1 in the Supporting Information).

*N-(3,5-Dimethoxyphenyl)-3-(isoquinolin-4-ylethynyl)-4-methylbenzamide (**8**). General Procedure for Syntheses of **8**−**15**, **42a**−**d** and **42f**.* To a solution of **41a** (100 mg, 0.25 mmol) in dry MeCN (20 mL) were added **39a** (76 mg, 0.34 mmol), CsF (95 mg, 0.63 mmol), and Et_3N (105 μL, 0.76 mmol) at rt under a N_2 atmosphere. The mixture was stirred at rt for 6 h. The resulting solution was poured into water and extracted with EtOAc. The organic layer was washed with brine and dried with Na_2SO_4 to give the crude product, which was purified by flash column chromatography (SiO_2, CH_2Cl_2/MeOH, 25:1) to give **8** as a white solid (91 mg, yield 85%); mp 177−178 °C. ^{1}H NMR (400 MHz, DMSO-d_6): δ 10.26 (s, 1H), 9.39 (s, 1H), 8.84 (s, 1H), 8.36 (d, *J* = 8.5 Hz, 1H), 8.28 (s, 1H), 8.25 (s, 1H), 8.00 (t, *J* = 7.6 Hz, 1H), 7.94 (d, *J* = 8.0 Hz, 1H), 7.83 (t, *J* = 7.5 Hz, 1H), 7.56 (d, *J* = 8.0 Hz, 1H), 7.11 (d, *J* = 2.0 Hz, 2H), 6.28 (s, 1H), 3.75 (s, 6H), 2.67 (s, 3H). ^{13}C NMR (126 MHz, DMSO-d_6): δ 164.46, 160.37, 152.66, 146.27, 143.51, 140.73, 134.41, 132.78, 132.10, 130.90, 129.97, 128.53, 128.50, 128.44, 127.43, 124.23, 121.84, 114.70, 98.58, 95.82, 94.63, 88.85, 55.11, 20.61. HRMS (ESI, *m*/*z*) for $C_{27}H_{22}N_2O_3$ [M + H]$^+$: calcd, 423.1703; found, 423.1723. HPLC analysis: 22.78 min, 98.92% purity.

*N-(3,5-Dimethoxyphenyl)-3-(imidazo[1,2-b]pyridazin-3-ylethynyl)-4-methylbenzamide (**9**).* It is obtained as a brown solid (yield 76%); mp 95−96 °C. ^{1}H NMR (400 MHz, DMSO-d_6): δ 10.26 (s, 1H), 8.73 (dd, *J* = 4.4, 1.4 Hz, 1H), 8.27 (dd, *J* = 9.2, 1.5 Hz, 1H), 8.24 (s, 1H), 8.18 (d, *J* = 1.8 Hz, 1H), 7.92 (dd, *J* = 8.0, 1.8 Hz, 1H), 7.53 (d, *J* = 8.1 Hz, 1H), 7.40 (dd, *J* = 9.2, 4.4 Hz, 1H), 7.11 (d, *J* = 2.2 Hz, 2H), 6.27 (t, *J* = 2.2 Hz, 1H), 3.74 (s, 6H), 2.60 (s, 3H). ^{13}C NMR (151 MHz, DMSO-d_6): δ 164.39, 160.38, 145.10, 143.25, 140.79, 139.67, 138.26, 132.67, 130.12, 130.03, 128.49, 126.14, 121.70, 119.11, 111.74, 98.54, 96.50, 95.83, 81.08, 55.14, 20.40. HRMS (ESI, *m*/*z*) for $C_{24}H_{20}N_4O_3$ [M + H]$^+$: calcd, 413.1608; found, 413.1604. HPLC analysis: 16.76 min, 98.41% purity.

*N-(3,5-Dimethoxyphenyl)-4-methyl-3-(pyridin-3-ylethynyl)-benzamide (**10**).* It is obtained as a yellow solid (yield 81%); mp 111−113 °C. ^{1}H NMR (400 MHz, DMSO-d_6): δ 10.22 (s, 1H), 8.82 (s, 1H), 8.62 (s, 1H), 8.16 (s, 1H), 8.04 (d, *J* = 7.5 Hz, 1H), 7.91 (d, *J* = 7.5 Hz, 1H), 7.51 (t, *J* = 8.1 Hz, 2H), 7.10 (s, 2H), 6.27 (s, 1H), 3.74 (s, 6H), 2.56 (s, 3H). ^{13}C NMR (151 MHz, DMSO-d_6): δ 164.41, 160.38, 151.61, 149.25, 143.67, 140.76, 138.60, 132.66, 130.67, 129.97, 128.55, 123.75, 121.62, 119.32, 98.51, 95.81, 90.64, 90.46, 55.13, 20.38. HRMS (ESI, *m*/*z*) for $C_{23}H_{20}N_2O_3$ [M + H]$^+$: calcd, 373.1547; found, 375.1543. HPLC analysis: 16.86 min, 99.18% purity.

*3-((2-Aminopyridin-3-yl)ethynyl)-N-(3,5-dimethoxyphenyl)-4-methylbenzamide (**11**).* It is obtained as a yellow solid (yield 85%); mp 179−180 °C. ^{1}H NMR (400 MHz, DMSO-d_6): δ 10.19 (s, 1H), 8.23 (d, *J* = 1.8 Hz, 1H), 8.01 (s, 1H), 7.85 (dd, *J* = 8.0, 1.9 Hz, 1H), 7.65 (dd, *J* = 7.5, 1.4 Hz, 1H), 7.47 (d, *J* = 8.1 Hz, 1H), 7.10 (t, *J* = 2.2 Hz, 2H), 6.61 (dd, *J* = 7.4, 4.9 Hz, 1H), 6.32 (s, 2H), 6.27 (t, *J* = 2.2 Hz, 1H), 3.74 (s, 6H), 2.54 (s, 3H). ^{13}C NMR (151 MHz, DMSO-d_6): δ 164.65, 160.38, 159.43, 148.51, 143.10, 140.70, 139.97, 132.59, 130.87, 129.66, 127.78, 122.52, 112.36, 98.49, 98.40, 95.73, 92.70, 90.03, 55.12, 20.51. HRMS (ESI, *m*/*z*) for $C_{23}H_{21}N_3O_3$ [M + H]$^+$: calcd, 388.1656; found, 388.1653. HPLC analysis: 11.94 min, 98.18% purity.

*3-((2-Amino-5-chloropyridin-3-yl)ethynyl)-N-(3,5-dimethoxyphenyl)-4-methylbenzamide (**12**).* It is obtained as a brown solid (yield 82%); mp 195−197 °C. ^{1}H NMR (400 MHz, DMSO-d_6): δ 10.20 (s, 1H), 8.25 (s, 1H), 8.03 (s, 1H), 7.86 (d, *J* = 8.0 Hz, 1H), 7.76 (s, 1H), 7.47 (d, *J* = 8.0 Hz, 1H), 7.09 (d, *J* = 2.0 Hz, 2H), 6.61 (s, 2H), 6.26 (s, 1H), 3.73 (s, 6H), 2.53 (s, 3H). ^{13}C NMR (126 MHz, DMSO-d_6): δ 164.67, 160.34, 158.08, 147.66, 146.55, 143.32, 140.73, 139.58, 138.77, 132.63, 131.11, 129.60, 127.98, 122.07, 98.49, 95.71, 93.64, 88.47, 55.08, 20.42. HRMS (ESI, *m*/*z*) for $C_{23}H_{20}ClN_3O_3$ [M + H]$^+$: calcd, 422.1266; found, 422.1265. HPLC analysis: 15.27 min, 100.00% purity.

*6-Amino-5-((5-((3,5-dimethoxyphenyl)carbamoyl)-2-methylphenyl)ethynyl)nicotinamide (**13**).* It is obtained as a light yellow solid (yield 72%); mp 253−254 °C. ^{1}H NMR (400 MHz, DMSO-d_6): δ 10.23 (s, 1H), 8.53 (d, *J* = 2.3 Hz, 1H), 8.29 (d, *J* = 1.8 Hz, 1H), 8.12 (d, *J* = 2.3 Hz, 1H), 7.88−7.82 (m, 2H), 7.48 (d, *J* = 8.1 Hz, 1H), 7.21 (s, 1H), 7.10 (d, *J* = 2.2 Hz, 2H), 6.93 (s, 2H), 6.27 (t, *J* = 2.2 Hz, 1H), 3.74 (s, 6H), 2.56 (s, 3H). ^{13}C NMR (151 MHz, DMSO-d_6): δ 166.06, 164.79, 160.75, 160.38, 149.24, 143.20, 140.83, 139.26, 132.67, 131.14, 129.64, 127.88, 122.36, 118.09, 99.97, 98.50, 95.73, 92.73, 89.30, 55.13, 20.50. HRMS (ESI, *m*/*z*) for $C_{24}H_{22}N_4O_4$ [M + H]$^+$: calcd, 431.1714; found, 431.1718. HPLC analysis: 13.21 min, 96.15% purity.

*6-Amino-5-((5-((3,5-dimethoxyphenyl)carbamoyl)-2-methylphenyl)ethynyl)-N-methylnicotinamide (**14**).* It is obtained as

https://dx.doi.org/10.1021/acs.jmedchem.9b01912
J. Med. Chem. XXXX, XXX, XXX−XXX

a brown solid (yield 80%); mp 262−265 °C. ^{1}H NMR (400 MHz, DMSO-d_6): δ 10.20 (s, 1H), 8.49 (d, J = 2.3 Hz, 1H), 8.30−8.26 (m, 2H), 8.08 (d, J = 2.2 Hz, 1H), 7.86 (dd, J = 8.1, 1.4 Hz, 1H), 7.48 (d, J = 8.1 Hz, 1H), 7.09 (d, J = 2.1 Hz, 2H), 6.91 (s, 2H), 6.27 (t, J = 2.0 Hz, 1H), 3.74 (s, 6H), 2.75 (d, J = 4.4 Hz, 3H), 2.56 (s, 3H). ^{13}C NMR (151 MHz, DMSO-d_6): δ 164.75, 164.70, 160.61, 160.37, 148.62, 143.16, 140.78, 138.69, 132.67, 131.10, 129.62, 127.84, 122.32, 118.41, 100.01, 98.49, 95.73, 92.75, 89.25, 55.11, 26.00, 20.48. HRMS (ESI, m/z) for $C_{25}H_{24}N_4O_4$ [M + H]$^+$: calcd, 445.1871; found, 445.1866. HPLC analysis: 14.05 min, 97.75% purity.

*Methyl 6-Amino-5-((5-((3,5-dimethoxyphenyl)carbamoyl)-2-methylphenyl)ethynyl)nicotinate (**15**).* It is obtained as a yellow solid (yield 78%); mp 231−232 °C. ^{1}H NMR (400 MHz, DMSO-d_6): δ 10.19 (s, 1H), 8.56 (s, 1H), 8.29 (s, 1H), 8.05 (d, J = 2.0 Hz, 1H), 7.86 (dd, J = 1.6, 8.1 Hz, 1H), 7.48 (d, J = 8.1 Hz, 1H), 7.29 (s, 2H), 7.10 (s, 1H), 7.09 (s, 1H), 6.27 (s, 1H), 3.80 (s, 3H), 3.74 (s, 6H), 2.55 (s, 3H). ^{13}C NMR (151 MHz, DMSO-d_6): δ 164.94, 164.75, 161.67, 160.37, 150.82, 143.31, 140.78, 140.35, 132.65, 131.25, 129.60, 127.96, 122.18, 113.73, 100.63, 98.49, 95.72, 93.06, 88.52, 55.11, 51.67, 20.47. HRMS (ESI, m/z) for $C_{25}H_{23}N_3O_5$ [M + H]$^+$: calcd, 446.1711; found, 446.1713. HPLC analysis: 18.44 min, 99.46% purity.

*3-((2-Amino-5-(1-methyl-1H-pyrazol-4-yl)pyridin-3-yl)ethynyl)-N-(3,5-dimethoxyphenyl)-4-methylbenzamide (**16**).* *General Procedure for Syntheses of **16**−**22**.* To a solution of **42a** (80 mg, 0.17 mmol) in toluene/EtOH/H_2O (2 mL, 2:1:1, v/v/v) were added 1-methyl-4-(4,4,5,5-tetramethyl-1,3,2-dioxaborolan-2-yl)-1*H*-pyrazole (71 mg, 0.34 mmol), $Pd(PPh_3)_4$ (19 mg, 0.017 mmol), and K_2CO_3 (59 mg, 0.43 mmol) at rt. After stirring for 5 min under a N_2 atmosphere, the mixture was irradiated at 100 °C for 20 min. The mixture was poured into water and extracted with EtOAc. The organic layer was separated, washed with brine, dried with anhydrous Na_2SO_4, filtered, and concentrated. The crude product was further purified by flash column chromatography (SiO_2, CH_2Cl_2/MeOH/NH_4OH, 20:1:0.02) to afford compound **16** as a light yellow solid (80 mg, yield 85%); mp 230−231 °C. ^{1}H NMR (400 MHz, DMSO-d_6): δ 10.20 (s, 1H), 8.27 (d, J = 2.3 Hz, 1H), 8.24 (d, J = 1.9 Hz, 1H), 8.08 (s, 1H), 7.89−7.83 (m, 2H), 7.83 (s, 1H), 7.48 (d, J = 8.1 Hz, 1H), 7.10 (d, J = 2.2 Hz, 2H), 6.29 (s, 2H), 6.27 (t, J = 2.2 Hz, 1H), 3.84 (s, 3H), 3.74 (s, 6H), 2.57 (s, 3H). ^{13}C NMR (126 MHz, DMSO-d_6): δ 164.72, 160.36, 157.83, 145.25, 143.10, 140.78, 136.30, 135.34, 132.64, 130.93, 129.64, 127.77, 126.82, 122.47, 118.70, 117.61, 101.10, 98.50, 95.73, 92.84, 89.92, 55.11, 38.62, 20.55. HRMS (ESI, m/z) for $C_{27}H_{25}N_5O_3$ [M + H]$^+$: calcd, 468.2030; found, 468.2028. HPLC analysis: 14.11 min, 99.65% purity.

*3-((2-Amino-5-(1-methyl-1H-pyrazol-4-yl)pyridin-3-yl)ethynyl)-N-(3,5-dimethoxyphenyl) benzamide (**17**).* It is obtained as a yellow solid (yield 77%); mp 221−222 °C. ^{1}H NMR (400 MHz, DMSO-d_6): δ 10.30 (s, 1H), 8.26 (d, J = 2.2 Hz, 1H), 8.23 (s, 1H), 8.07 (s, 1H), 7.93 (d, J = 7.9 Hz, 1H), 7.89−7.83 (m, 2H), 7.81 (s, 1H), 7.58 (t, J = 7.8 Hz, 1H), 7.10 (t, J = 2.1 Hz, 2H), 6.44 (s, 2H), 6.28 (t, J = 2.1 Hz, 1H), 3.83 (s, 3H), 3.72 (d, J = 10.1 Hz, 6H). ^{13}C NMR (101 MHz, DMSO-d_6): δ 164.92, 160.40, 157.94, 145.12, 140.75, 136.48, 135.36, 134.22, 130.53, 128.82, 127.80, 126.80, 122.74, 118.72, 117.47, 100.86, 98.52, 98.43, 95.81, 94.05, 86.26, 55.15, 38.67. HRMS (ESI, m/z) for $C_{26}H_{23}N_5O_3$ [M + H]$^+$: calcd, 454.1874; found, 454.1869. HPLC analysis: 2.93 min, 99.16% purity.

*3-((2-Amino-5-(1-methyl-1H-pyrazol-4-yl)pyridin-3-yl)ethynyl)-N-(3,5-dimethoxyphenyl)-4-isopropylbenzamide (**18**).* It is obtained as a bright yellow solid (yield 80%); mp 216−217 °C. ^{1}H NMR (400 MHz, DMSO-d_6): δ 10.22 (s, 1H), 8.28 (s, 1H), 8.25 (s, 1H), 8.09 (s, 1H), 7.91 (d, J = 7.9 Hz, 1H), 7.83 (s, 2H), 7.54 (d, J = 8.1 Hz, 1H), 7.11 (s, 2H), 6.28 (d, J = 6.4 Hz, 3H), 3.85 (s, 3H), 3.74 (s, 6H), 3.62−3.52 (m, 1H), 1.31 (d, J = 6.7 Hz, 6H). ^{13}C NMR (151 MHz, DMSO-d_6): δ 164.87, 160.41, 157.87, 153.00, 145.29, 140.85, 136.26, 135.41, 132.79, 131.54, 128.28, 126.90, 125.30, 121.40, 118.71, 117.66, 101.19, 98.47, 95.73, 92.59, 89.56, 55.14, 38.64, 31.33, 22.81. HRMS (ESI, m/z) for $C_{29}H_{29}N_5O_3$ [M + H]$^+$: calcd, 496.2343; found, 496.2343. HPLC analysis: 16.51 min, 99.31% purity.

*3-((2-Amino-5-(1-methyl-1H-pyrazol-4-yl)pyridin-3-yl)ethynyl)-N-(3,5-dimethoxyphenyl)-4-methoxybenzamide (**19**).* It is obtained as a yellow solid (yield 75%); mp 229−230 °C. ^{1}H NMR (400 MHz, DMSO-d_6): δ 10.13 (s, 1H), 8.27 (d, J = 2.4 Hz, 1H), 8.22 (d, J = 2.3 Hz, 1H), 8.08 (s, 1H), 8.01 (dd, J = 8.8, 2.3 Hz, 1H), 7.83 (d, J = 0.6 Hz, 1H), 7.79 (d, J = 2.4 Hz, 1H), 7.26 (d, J = 8.9 Hz, 1H), 7.10 (s, 1H), 7.09 (s, 1H), 6.30 (s, 2H), 6.26 (t, J = 2.3 Hz, 1H), 3.98 (s, 3H), 3.84 (s, 3H), 3.74 (s, 6H). ^{13}C NMR (101 MHz, DMSO-d_6): δ 164.26, 161.82, 160.37, 157.97, 154.39, 145.16, 140.92, 135.40, 135.28, 131.87, 130.29, 127.06, 126.85, 118.75, 117.60, 111.12, 101.24, 98.44, 95.64, 91.14, 90.04, 56.34, 55.13, 38.67. HRMS (ESI, m/z) for $C_{27}H_{25}N_5O_4$ [M + H]$^+$: calcd, 484.1908; found, 484.0693. HPLC analysis: 22.50 min, 100.00% purity.

*3-((2-Amino-5-(1-methyl-1H-pyrazol-4-yl)pyridin-3-yl)ethynyl)-N-(3,5-dimethoxyphenyl)-4-fluorobenzamide (**20**).* It is obtained as a yellow solid (yield 88%); mp 236−238 °C. ^{1}H NMR (400 MHz, DMSO-d_6): δ 10.28 (s, 1H), 8.39 (d, J = 6.9 Hz, 1H), 8.29 (s, 1H), 8.09 (s, 1H), 8.03−7.97 (m, 1H), 7.83 (d, J = 2.8 Hz, 2H), 7.51 (t, J = 9.4 Hz, 1H), 7.07 (s, 2H), 6.40 (s, 2H), 6.28 (s, 1H), 3.84 (s, 3H), 3.74 (s, 6H). ^{13}C NMR (126 MHz, DMSO-d_6): δ 163.88, 162.23 (d, J = 254.5 Hz), 160.38, 157.99, 145.72, 140.61, 136.25, 135.35, 133.22, 131.59 (d, J = 2.9 Hz), 130.42 (d, J = 9.1 Hz), 126.85, 118.59, 117.57, 115.77 (d, J = 21.6 Hz), 110.98 (d, J = 16.2 Hz), 100.27, 98.55, 95.86, 91.15 (d, J = 2.3 Hz), 87.27, 55.12, 38.61. ^{19}F NMR (376 MHz, DMSO-d_6): δ −106.42 to −106.54 (m). HRMS (ESI, m/z) for $C_{26}H_{22}FN_5O_3$ [M + H]$^+$: calcd, 472.1780; found, 472.1776. HPLC analysis: 14.02 min, 98.35% purity.

*3-((2-Amino-5-(1-methyl-1H-pyrazol-4-yl)pyridin-3-yl)ethynyl)-4-chloro-N-(3,5-dimethoxyphenyl)benzamide (**21**).* It is obtained as a light yellow solid (yield 75%); mp 229−230 °C. ^{1}H NMR (400 MHz, DMSO-d_6): δ 10.34 (s, 1H), 8.39 (d, J = 2.0 Hz, 1H), 8.31 (d, J = 2.1 Hz, 1H), 8.10 (s, 1H), 7.94 (dd, J = 8.4, 2.0 Hz, 1H), 7.85 (d, J = 2.2 Hz, 1H), 7.83 (s, 1H), 7.77 (d, J = 8.4 Hz, 1H), 7.08 (s, 2H), 6.39 (s, 2H), 6.29 (s, 1H), 3.84 (s, 3H), 3.74 (s, 6H). ^{13}C NMR (101 MHz, DMSO-d_6): δ 160.41, 158.92, 158.05, 145.98, 140.46, 137.21, 136.26, 135.38, 133.94, 132.52, 129.42, 129.19, 126.91, 122.26, 118.59, 117.66, 98.55, 98.46, 95.92, 91.36, 90.90, 55.16, 38.66. HRMS (ESI, m/z) for $C_{26}H_{22}ClN_5O_3$ [M + H]$^+$: calcd, 488.1484; found, 488.1484. HPLC analysis: 15.57 min, 97.94% purity.

*3-((2-Amino-5-(1-methyl-1H-pyrazol-4-yl)pyridin-3-yl)ethynyl)-N-(3,5-dimethoxyphenyl)-4-(trifluoromethyl)benzamide (**22**).* It is obtained as a bright yellow solid (yield 83%); mp 223−224 °C. ^{1}H NMR (400 MHz, DMSO-d_6): δ 10.49 (s, 1H), 8.50 (s, 1H), 8.32 (s, 1H), 8.10 (s, 1H), 8.07 (d, J = 8.0 Hz, 1H), 7.99 (d, J = 8.1 Hz, 1H), 7.82 (s, 1H), 7.76 (s, 1H), 7.09 (s, 2H), 6.40 (s, 2H), 6.31 (s, 1H), 3.85 (s, 3H), 3.75 (s, 6H). ^{13}C NMR (126 MHz, DMSO-d_6): δ 163.83, 160.43, 158.03, 146.29, 140.37, 138.79, 136.34, 135.32, 133.15, 131.22 (q, J = 29.8 Hz), 127.86, 126.92, 126.43 (q, J = 4.5 Hz), 123.40 (q, J = 273.4 Hz), 120.63, 118.47, 117.71, 99.97, 98.62, 96.11, 91.74, 89.99, 55.15, 38.59. ^{19}F NMR (471 MHz, DMSO-d_6): δ −60.95 (s). HRMS (ESI, m/z) for $C_{27}H_{22}F_3N_5O_3$ [M + H]$^+$: calcd, 522.1748; found, 522.1745. HPLC analysis: 16.56 min, 98.15% purity.

*3-((2-Amino-5-(1-methyl-1H-pyrazol-4-yl)pyridin-3-yl)ethynyl)-4-methyl-N-phenylbenzamide (**23**).* *General Procedure for Syntheses of **23**−**33**, **38f**−**g**, **41a**−**g**, and **48a**−**c**.* To a solution of **45** (100 mg, 0.30 mmol) in DMF (3 mL) were added HATU (148 mg, 0.39 mmol) and DIPEA (149 μL, 0.90 mmol) at rt, and after stirring for 30 min, aniline (30 μL, 0.33 mmol) was added, and the mixture was stirred at rt for 4 h. The resulting solution was poured into water and extracted with EtOAc. The organic layer was washed with water and brine and dried with Na_2SO_4. The resultant crude material was purified by flash column chromatography (SiO_2, CH_2Cl_2/MeOH/NH_4OH, 20:1:0.02) to give **23** as a yellow solid (116 mg, yield 95%); mp 95−96 °C. ^{1}H NMR (400 MHz, DMSO-d_6): δ 10.29 (s, 1H), 8.32−8.24 (m, 2H), 8.08 (s, 1H), 7.90−7.85 (m, 2H), 7.83 (s, 1H), 7.79 (d, J = 7.7 Hz, 2H), 7.49 (d, J = 8.0 Hz, 1H), 7.36 (t, J = 7.9 Hz, 2H), 7.11 (t, J = 7.4 Hz, 1H), 6.31 (s, 2H), 3.84 (s, 3H), 2.57 (s, 3H). ^{13}C NMR (151 MHz, DMSO-d_6): δ 164.70, 157.85, 145.26, 143.04, 139.12, 136.32, 135.36, 132.71, 131.00, 129.64, 128.62, 127.80, 126.83, 123.69, 122.49, 120.35, 118.72, 117.62, 101.13, 92.88, 89.91, 38.62, 20.55.

https://dx.doi.org/10.1021/acs.jmedchem.9b01912
J. Med. Chem. XXXX, XXX, XXX−XXX

HRMS (ESI, m/z) for $C_{25}H_{21}N_5O$ $[M + H]^+$: calcd, 408.1819; found, 408.1820. HPLC analysis: 13.18 min, 98.93% purity.

*3-((2-Amino-5-(1-methyl-1H-pyrazol-4-yl)pyridin-3-yl)ethynyl)-N-(2-methoxyphenyl)-4-methylbenzamide (**24**).* It is obtained as a brown solid (yield 90%); mp 107−108 °C. ^{1}H NMR (400 MHz, DMSO-d_6): δ 9.48 (s, 1H), 8.30−8.23 (m, 2H), 8.08 (s, 1H), 7.87 (t, J = 6.5 Hz, 2H), 7.83 (s, 1H), 7.75 (d, J = 7.3 Hz, 1H), 7.48 (d, J = 8.0 Hz, 1H), 7.19 (t, J = 7.3 Hz, 1H), 7.10 (d, J = 7.8 Hz, 1H), 6.98 (t, J = 7.6 Hz, 1H), 6.31 (s, 2H), 3.84 (br s, 6H), 2.57 (s, 3H). ^{13}C NMR (126 MHz, DMSO-d_6): δ 164.23, 157.84, 151.62, 145.25, 143.06, 136.33, 135.35, 132.28, 130.91, 129.71, 127.56, 126.83, 126.71, 125.84, 124.56, 122.58, 120.19, 118.71, 117.61, 111.44, 101.13, 92.84, 89.90, 55.71, 38.61, 20.53. HRMS (ESI, m/z) for $C_{26}H_{23}N_5O_2$ $[M + H]^+$: calcd, 438.1925; found, 438.1923. HPLC analysis: 14.03 min, 98.47% purity.

*3-((2-Amino-5-(1-methyl-1H-pyrazol-4-yl)pyridin-3-yl)ethynyl)-N-(3-methoxyphenyl)-4-methylbenzamide (**25**).* It is obtained as a yellow solid (yield 86%); mp 232−233 °C. ^{1}H NMR (400 MHz, DMSO-d_6): δ 10.26 (s, 1H), 8.28 (s, 1H), 8.27 (s, 1H), 8.08 (s, 1H), 7.86 (t, J = 10.0 Hz, 3H), 7.48 (d, J = 8.5 Hz, 2H), 7.41 (d, J = 8.1 Hz, 1H), 7.26 (t, J = 8.1 Hz, 1H), 6.69 (d, J = 6.9 Hz, 1H), 6.32 (s, 2H), 3.85 (s, 3H), 3.76 (s, 3H), 2.57 (s, 3H). ^{13}C NMR (151 MHz, DMSO-d_6): δ 164.74, 159.45, 157.87, 145.28, 143.10, 140.33, 136.34, 135.38, 132.71, 131.00, 129.66, 129.41, 127.82, 126.84, 122.51, 118.75, 117.66, 112.57, 109.18, 106.07, 101.17, 92.91, 89.94, 55.01, 38.62, 20.56. HRMS (ESI, m/z) for $C_{26}H_{23}N_5O_2$ $[M + H]^+$: calcd, 438.1925; found, 438.1925. HPLC analysis: 13.60 min, 98.64% purity.

*3-((2-Amino-5-(1-methyl-1H-pyrazol-4-yl)pyridin-3-yl)ethynyl)-N-(4-methoxyphenyl)-4-methylbenzamide (**26**).* It is obtained as a light yellow solid (yield 91%); mp 180−182 °C. ^{1}H NMR (400 MHz, DMSO-d_6): δ 10.17 (s, 1H), 8.27 (d, J = 1.9 Hz, 1H), 8.24 (s, 1H), 8.09 (s, 1H), 7.86 (d, J = 8.1 Hz, 2H), 7.83 (s, 1H), 7.68 (d, J = 8.8 Hz, 2H), 7.47 (d, J = 8.0 Hz, 1H), 6.93 (d, J = 8.9 Hz, 2H), 6.31 (s, 2H), 3.84 (s, 3H), 3.75 (s, 3H), 2.56 (s, 3H). ^{13}C NMR (126 MHz, DMSO-d_6): δ 164.21, 157.81, 155.54, 145.22, 142.82, 136.28, 135.33, 132.76, 132.14, 130.87, 129.59, 127.67, 126.81, 122.42, 121.92, 118.69, 117.61, 113.73, 101.13, 92.90, 89.81, 55.16, 38.60, 20.50. HRMS (ESI, m/z) for $C_{26}H_{23}N_5O_2$ $[M + H]^+$: calcd, 438.1925; found, 438.1925. HPLC analysis: 3.16 min, 99.72% purity.

*3-((2-Amino-5-(1-methyl-1H-pyrazol-4-yl)pyridin-3-yl)ethynyl)-N-(2-chlorophenyl)-4-methylbenzamide (**27**).* It is obtained as a yellow solid (yield 75%); mp 175−176 °C. ^{1}H NMR (400 MHz, DMSO-d_6): δ 10.12 (s, 1H), 8.28−8.26 (m, 2H), 8.09 (s, 1H), 7.91 (dd, J = 1.2, 7.7 Hz, 2H), 7.86 (d, J = 2.0 Hz, 1H), 7.83 (s, 1H), 7.59−7.55 (m, 2H), 7.50 (d, J = 8.1 Hz, 1H), 7.40 (t, J = 7.6 Hz, 1H), 7.31 (t, J = 7.6 Hz, 1H), 6.31 (s, 2H), 3.84 (s, 3H), 2.57 (s, 3H). ^{13}C NMR (126 MHz, DMSO-d_6): δ 164.58, 157.81, 145.25, 143.34, 136.31, 135.33, 135.01, 131.71, 131.06, 129.72, 129.56, 128.50, 127.72, 127.51, 127.47, 126.81, 122.61, 118.68, 117.62, 101.08, 92.75, 89.92, 38.59, 20.54. HRMS (ESI, m/z) for $C_{25}H_{20}ClN_5O$ $[M + H]^+$: calcd, 442.1429; found, 442.1426. HPLC analysis: 14.08 min, 98.06% purity.

*3-((2-Amino-5-(1-methyl-1H-pyrazol-4-yl)pyridin-3-yl)ethynyl)-N-(3-chlorophenyl)-4-methylbenzamide (**28**).* It is obtained as a yellow solid (yield 85%); mp 204−206 °C. ^{1}H NMR (400 MHz, DMSO-d_6): δ 10.45 (s, 1H), 8.27 (d, J = 2.3 Hz, 1H), 8.26 (d, J = 1.7 Hz, 1H), 8.08 (s, 1H), 7.98 (t, J = 1.9 Hz, 1H), 7.89−7.85 (m, 2H), 7.83 (s, 1H), 7.73 (dd, J = 7.9, 1.3 Hz, 1H), 7.50 (d, J = 8.0 Hz, 1H), 7.39 (t, J = 8.1 Hz, 1H), 7.17 (dd, J = 7.9, 1.8 Hz, 1H), 6.31 (s, 2H), 3.84 (s, 3H), 2.57 (s, 3H). ^{13}C NMR (126 MHz, DMSO-d_6): δ 164.97, 157.85, 145.29, 143.37, 140.61, 136.32, 135.35, 132.94, 132.30, 131.02, 130.35, 129.72, 127.84, 126.83, 123.37, 122.57, 119.68, 118.70, 118.60, 117.62, 101.07, 92.77, 90.01, 38.62, 20.57. HRMS (ESI, m/z) for $C_{25}H_{20}ClN_5O$ $[M + H]^+$: calcd, 442.1429; found, 442.1429. HPLC analysis: 15.62 min, 96.20% purity.

*3-((2-Amino-5-(1-methyl-1H-pyrazol-4-yl)pyridin-3-yl)ethynyl)-N-(4-chlorophenyl)-4-methylbenzamide (**29**).* It is obtained as a yellow solid (yield 90%); mp 225−226 °C. ^{1}H NMR (400 MHz, DMSO-d_6): δ 10.40 (s, 1H), 8.27 (d, J = 2.4 Hz, 1H), 8.25 (d, J = 1.8 Hz, 1H), 8.08 (s, 1H), 7.87 (dd, J = 8.1, 1.8 Hz, 1H), 7.85 (d, J = 2.4 Hz, 1H), 7.84−7.80 (m, 3H), 7.49 (d, J = 8.1 Hz, 1H), 7.44−7.39 (m, 2H), 6.29 (s, 2H), 3.84 (s, 3H), 2.57 (s, 3H). ^{13}C NMR (126 MHz, DMSO-d_6): δ 164.78, 157.82, 145.26, 143.21, 138.08, 136.30, 135.33, 132.42, 130.98, 129.67, 128.52, 127.79, 127.27, 126.80, 122.52, 121.81, 118.69, 117.61, 101.07, 92.78, 89.96, 38.59, 20.53. HRMS (ESI, m/z) for $C_{25}H_{20}ClN_5O$ $[M + H]^+$: calcd, 442.1429; found, 442.1425. HPLC analysis: 15.48 min, 99.00% purity.

*3-((2-Amino-5-(1-methyl-1H-pyrazol-4-yl)pyridin-3-yl)ethynyl)-4-methyl-N-(3-(trifluoromethyl)phenyl)benzamide (**30**).* It is obtained as a deep yellow solid (yield 85%); mp 206−208 °C. ^{1}H NMR (400 MHz, DMSO-d_6): δ 10.63 (s, 1H), 8.30 (d, J = 1.8 Hz, 1H), 8.27 (d, J = 2.4 Hz, 1H), 8.26 (s, 1H), 8.09 (d, J = 9.3 Hz, 2H), 7.91 (dd, J = 8.0, 1.9 Hz, 1H), 7.86 (d, J = 2.4 Hz, 1H), 7.82 (d, J = 0.6 Hz, 2H), 7.61 (t, J = 8.0 Hz, 1H), 7.51 (d, J = 8.1 Hz, 1H), 7.46 (d, J = 7.8 Hz, 1H), 6.30 (s, 2H), 3.85 (s, 3H), 2.58 (s, 3H). ^{13}C NMR (126 MHz, DMSO-d_6): δ 165.21, 157.84, 145.28, 143.43, 142.87, 136.32, 135.34, 132.26, 131.12, 129.75, 129.70, 129.61, 127.93, 126.81, 125.90 (q, J = 3.8 Hz), 124.39 (q, J = 271.3 Hz), 123.57 (q, J = 32.0 Hz), 122.56, 120.14, 118.69, 117.61, 101.06, 92.75, 90.02, 38.60, 20.56. ^{19}F NMR (471 MHz, DMSO-d_6): δ −61.28. HRMS (ESI, m/z) for $C_{26}H_{20}F_3N_5O$ $[M + H]^+$: calcd, 476.1693; found, 476.1693. HPLC analysis: 16.28 min, 96.39% purity.

*3-((2-Amino-5-(1-methyl-1H-pyrazol-4-yl)pyridin-3-yl)ethynyl)-4-methyl-N-(4-(trifluoromethyl)phenyl)benzamide (**31**).* It is obtained as a yellow solid (yield 90%); mp 239−240 °C. ^{1}H NMR (400 MHz, DMSO-d_6): δ 10.66 (s, 1H), 8.29 (d, J = 1.4 Hz, 1H), 8.27 (d, J = 2.2 Hz, 1H), 8.08 (s, 1H), 8.03 (d, J = 8.5 Hz, 2H), 7.90 (dd, J = 7.9, 1.5 Hz, 1H), 7.85 (d, J = 2.2 Hz, 1H), 7.82 (s, 1H), 7.73 (d, J = 8.6 Hz, 2H), 7.50 (d, J = 8.0 Hz, 1H), 6.30 (s, 2H), 3.84 (s, 3H), 2.58 (s, 3H). ^{13}C NMR (126 MHz, DMSO-d_6): δ 165.09, 157.84, 145.29, 143.43, 139.95, 136.31, 135.34, 132.17, 131.05, 129.86, 129.74, 129.33 (q, J = 31.5 Hz), 127.87, 126.82, 124.16 (q, J = 272.2 Hz), 123.76, 122.57, 119.93 (q, J = 3.7 Hz), 118.70, 117.62, 116.36 (q, J = 4.1 Hz), 101.07, 92.76, 90.00, 38.60, 20.56. ^{19}F NMR (471 MHz, DMSO-d_6): δ −60.31. HRMS (ESI, m/z) for $C_{26}H_{20}F_3N_5O$ $[M + H]^+$: calcd, 476.1693; found, 476.1694. HPLC analysis: 16.85 min, 98.52% purity.

*3-((2-Amino-5-(1-methyl-1H-pyrazol-4-yl)pyridin-3-yl)ethynyl)-N-(2,4-dichlorophenyl)-4-methylbenzamide (**32**).* It is obtained as a light yellow solid (yield 75%); mp 196−198 °C. ^{1}H NMR (400 MHz, DMSO-d_6): δ 10.18 (s, 1H), 8.27 (d, J = 1.9 Hz, 2H), 8.08 (s, 1H), 7.90 (dd, J = 8.0, 2.0 Hz, 1H), 7.85 (d, J = 2.4 Hz, 1H), 7.75 (d, J = 2.3 Hz, 1H), 7.61 (d, J = 8.6 Hz, 1H), 7.54−7.45 (m, 2H), 6.30 (s, 2H), 3.84 (s, 3H), 2.57 (s, 3H). ^{13}C NMR (126 MHz, DMSO-d_6): δ 164.66, 157.83, 145.28, 143.53, 136.33, 135.34, 134.25, 131.46, 131.11, 130.82, 130.57, 129.76, 129.60, 129.07, 127.77, 127.65, 126.82, 122.65, 118.69, 117.61, 101.06, 92.71, 89.99, 38.61, 20.58. HRMS (ESI, m/z) for $C_{25}H_{19}Cl_2N_5O$ $[M + H]^+$: calcd, 476.1040; found, 476.1035. HPLC analysis: 16.58 min, 97.87% purity.

*3-((2-Amino-5-(1-methyl-1H-pyrazol-4-yl)pyridin-3-yl)ethynyl)-N-(3,4-dichlorophenyl)-4-methylbenzamide (**33**).* It is obtained as a yellow solid (yield 82%); mp 108−111 °C. ^{1}H NMR (400 MHz, DMSO-d_6): δ 10.59 (s, 1H), 8.27 (s, 2H), 8.18 (s, 1H), 8.08 (s, 1H), 7.92−7.84 (m, 2H), 7.84−7.74 (m, 2H), 7.63 (d, J = 8.8 Hz, 1H), 7.50 (d, J = 7.5 Hz, 1H), 6.31 (s, 2H), 3.84 (s, 3H), 2.57 (s, 3H). ^{13}C NMR (126 MHz, DMSO-d_6): δ 165.02, 157.84, 145.30, 143.51, 139.29, 136.32, 135.34, 132.04, 131.05, 130.84, 130.57, 129.75, 127.86, 126.82, 125.11, 122.59, 121.42, 120.23, 118.69, 117.62, 101.04, 92.72, 90.04, 38.61, 20.56. HRMS (ESI, m/z) for $C_{25}H_{19}Cl_2N_5O$ $[M + H]^+$: calcd, 476.1040; found, 476.1042. HPLC analysis: 9.59 min, 98.70% purity.

*4-((2-Amino-5-(1-methyl-1H-pyrazol-4-yl)pyridin-3-yl)ethynyl)-N-(4-chlorophenyl)-3-methylbenzamide (**34**).* *General Procedure for Syntheses of **34**−**37**.* Step 1: The cross-coupling product was prepared in 69% yield from **48a** and **39i** according to the procedure in the preparation of **8**. Step 2: According to the general procedure in the preparation of **16**, the title compound (**34**) was prepared in 89% yield as a yellow solid; mp 224−225 °C. ^{1}H NMR (400 MHz, DMSO-d_6): δ 10.44 (s, 1H), 8.28 (s, 1H), 8.09 (s, 1H), 7.91 (s, 1H), 7.88−7.78 (m, 6H), 7.42 (d, J = 8.4 Hz, 2H), 6.32 (s, 2H), 3.84 (s, 3H), 2.58 (s,

https://dx.doi.org/10.1021/acs.jmedchem.9b01912
J. Med. Chem. XXXX, XXX, XXX−XXX

3H). ^{13}C NMR (126 MHz, DMSO-d_6): δ 164.98, 157.83, 145.46, 139.50, 138.07, 136.40, 135.34, 134.11, 131.71, 128.68, 128.52, 127.31, 126.82, 125.64, 125.11, 121.86, 118.66, 117.63, 100.95, 92.90, 91.57, 38.60, 20.53. HRMS (ESI, m/z) for $C_{25}H_{20}ClN_5O$ [M + H]$^+$: calcd, 442.1429; found, 442.1428. HPLC analysis: 5.57 min, 100.00% purity.

*N-(3-((2-Amino-5-(1-methyl-1H-pyrazol-4-yl)pyridin-3-yl)-ethynyl)-4-methylphenyl)-4-chlorobenzamide (**35**).* It is obtained as a yellow solid (yield 76%); mp 190−191 °C. ^{1}H NMR (400 MHz, DMSO-d_6): δ 10.36 (s, 1H), 8.26 (d, J = 2.3 Hz, 1H), 8.09 (s, 1H), 8.05 (d, J = 2.3 Hz, 1H), 8.00 (d, J = 8.5 Hz, 2H), 7.85 (d, J = 2.3 Hz, 1H), 7.83 (s, 1H), 7.65−7.61 (m, 3H), 7.31 (d, J = 8.4 Hz, 1H), 6.20 (s, 2H), 3.84 (s, 3H), 2.46 (s, 3H). ^{13}C NMR (151 MHz, DMSO-d_6): δ 164.36, 157.77, 145.03, 136.71, 136.50, 136.20, 135.39, 134.93, 133.42, 129.83, 129.62, 128.54, 126.87, 123.51, 122.33, 121.10, 118.73, 117.72, 109.53, 101.43, 93.49, 89.02, 39.94, 39.80, 39.66, 39.52, 39.38, 39.24, 39.10, 38.64, 20.00. HRMS (ESI, m/z) for $C_{25}H_{20}ClN_5O$ [M + H]$^+$: calcd, 442.1429; found, 442.1429. HPLC analysis: 14.72 min, 95.77% purity.

*3-((2-Amino-5-(1-methyl-1H-pyrazol-4-yl)pyridin-3-yl)ethynyl)-N-(4-chlorophenyl)-N,4-dimethylbenzamide (**36**).* It is obtained as a deep yellow solid (yield 80%); mp 109−111 °C. ^{1}H NMR (600 MHz, DMSO-d_6): δ 8.25 (d, J = 2.4 Hz, 1H), 8.06 (s, 1H), 7.80 (d, J = 0.4 Hz, 1H), 7.79 (d, J = 2.3 Hz, 1H), 7.67 (d, J = 1.3 Hz, 1H), 7.37−7.35 (m, 2H), 7.24 (d, J = 8.7 Hz, 2H), 7.16 (d, J = 8.0 Hz, 1H), 7.06 (d, J = 7.8 Hz, 1H), 6.23 (s, 2H), 3.84 (s, 3H), 3.36 (s, 3H), 2.41 (s, 3H). ^{13}C NMR (126 MHz, DMSO-d_6): δ 168.66, 157.76, 145.20, 143.36, 140.91, 136.29, 135.32, 133.81, 131.73, 130.77, 129.09, 128.89, 128.81, 128.05, 126.80, 122.22, 118.68, 117.57, 101.08, 92.64, 89.76, 38.59, 37.83, 20.29. HRMS (ESI, m/z) for $C_{26}H_{22}ClN_5O$ [M + H]$^+$: calcd, 456.1586; found, 456.1583. HPLC analysis: 14.21 min, 98.57% purity.

*3-((5-(((4-Chlorophenyl)amino)methyl)-2-methylphenyl)-ethynyl)-5-(1-methyl-1H-pyrazol-4-yl)pyridin-2-amine (**37**).* It is obtained as a brown solid (yield 70%); mp 230−231 °C. ^{1}H NMR (500 MHz, DMSO-d_6): δ 8.24 (s, 1H), 8.07 (s, 1H), 7.82 (s, 2H), 7.60 (s, 1H), 7.27 (s, 2H), 7.06 (d, J = 7.4 Hz, 2H), 6.56 (d, J = 7.8 Hz, 2H), 6.46 (s, 1H), 6.22 (s, 2H), 4.23 (s, 2H), 3.84 (s, 3H), 2.45 (s, 3H). ^{13}C NMR (126 MHz, DMSO-d_6): δ 157.53, 147.41, 137.83, 137.50, 136.33, 135.37, 130.39, 129.58, 128.54, 127.63, 126.87, 122.17, 119.07, 118.63, 117.68, 113.66, 101.68, 93.75, 88.91, 45.86, 40.02, 39.85, 39.69, 39.52, 39.35, 39.19, 39.02, 38.61, 20.12. HRMS (ESI, m/z) for $C_{25}H_{22}ClN_5$ [M + H]$^+$: calcd, 428.1637; found, 428.1632. HPLC analysis: 17.79 min, 97.09% purity.

*6-Amino-5-bromonicotinamide (**38f**).* It is obtained as a deep brown solid (1.6 g, yield 80%). ^{1}H NMR (400 MHz, DMSO-d_6): δ 8.47 (d, J = 2.0 Hz, 1H), 8.15 (d, J = 2.0 Hz, 1H), 7.79 (s, 1H), 7.21 (s, 1H), 6.81 (s, 2H). MS (ESI) m/z: 217.1 [M + H]$^+$.

*6-Amino-5-bromo-N-methylnicotinamide (**38g**).* It is obtained as a brown solid (yield 91%). ^{1}H NMR (400 MHz, DMSO-d_6): δ 8.44 (d, J = 2.1 Hz, 1H), 8.26 (q, J = 4.5 Hz, 1H), 8.13 (d, J = 2.1 Hz, 1H), 6.79 (s, 2H), 2.68 (brs, 3H). MS (ESI) m/z: 231.3 [M + H]$^+$.

*4-((Trimethylsilyl)ethynyl)isoquinoline (**39a**).* *General Procedure for Syntheses of **39a−b** and **39f−h**.* To a solution of 4-bromoisoquinoline (2.0 g, 9.61 mmol) in dry MeCN/Et_3N (50 mL, 4:1, v/v) were added $Pd(PPh_3)_2Cl_2$ (337 mg, 0.48 mmol), CuI (183 mg, 0.96 mmol), and ethynyltrimethylsilane (2.0 mL, 14.42 mmol) at rt under a N_2 atmosphere. After stirring at 80 °C for 4 h under a nitrogen atmosphere, the mixture was diluted with EtOAc and filtered through a pad of Celite. The filtrate was removed by reduced pressure to give the crude material, which was further purified by flash column chromatography (SiO_2, petroleum ether/EtOAc, 15:1) to give **39a** as a light brown solid (1.7 g, yield 79%). ^{1}H NMR (400 MHz, DMSO-d_6): δ 9.34 (s, 1H), 8.66 (s, 1H), 8.21 (d, J = 8.2 Hz, 1H), 8.14 (dd, J = 1.0, 8.4 Hz, 1H), 7.94 (ddd, J = 1.3, 6.9, 8.3 Hz, 1H), 7.78 (ddd, J = 1.2, 6.9, 8.1 Hz, 1H), 0.32 (s, 9H). MS (ESI) m/z: 226.3 [M + H]$^+$.

*3-((Trimethylsilyl)ethynyl)imidazo[1,2-b]pyridazine (**39b**).* It is obtained as a brown solid (yield 82%). ^{1}H NMR (400 MHz, DMSO-d_6): δ 8.67 (dd, J = 1.3, 4.4 Hz, 1H), 8.21 (dd, J = 1.4, 9.2 Hz, 1H), 8.12 (s, 1H), 7.36 (dd, J = 4.4, 9.2 Hz, 1H), 0.27 (s, 9H). MS (ESI) m/z: 216.3 [M + H]$^+$.

*3-((Trimethylsilyl)ethynyl)pyridine (**39c**).* *General Procedure for Syntheses of **39c−e** and **39i**.* To a solution of 3-iodopyridine (2.0 g, 9.76 mmol) in dry Et_3N (50 mL) were added $Pd(PPh_3)_2Cl_2$ (342 mg, 0.49 mmol), CuI (186 mg, 0.98 mmol), and ethynyltrimethylsilane (2.1 mL, 14.63 mmol) at rt under a N_2 atmosphere. After stirring for 4 h, the mixture was diluted with EtOAc and filtered through a pad of Celite. The filtrate was removed by reduced pressure to give the crude product, which was further purified by column chromatography (SiO_2, petroleum ether/EtOAc, 15:1) to give **39c** as a light yellow solid (1.4 g, yield 82%). ^{1}H NMR (400 MHz, Chloroform-d): δ 8.69 (d, J = 1.1 Hz, 1H), 8.52 (dd, J = 4.8, 1.4 Hz, 1H), 7.77−7.69 (m, 1H), 7.23 (dd, J = 7.8, 4.9 Hz, 1H), 0.27 (s, 9H). MS (ESI) m/z: 226.3 [M + H]$^+$.

*3-((Trimethylsilyl)ethynyl)pyridin-2-amine (**39d**).* It is obtained as a yellow solid (yield 85.0%). ^{1}H NMR (400 MHz, DMSO-d_6): δ 7.95 (dd, J = 1.9, 4.9 Hz, 1H), 7.50 (dd, J = 1.9, 7.5 Hz, 1H), 6.52 (dd, J = 4.9, 7.5 Hz, 1H), 6.10 (s, 2H). MS (ESI) m/z: 191.1 [M + H]$^+$.

*5-Chloro-3-((trimethylsilyl)ethynyl)pyridin-2-amine (**39e**).* It is obtained as a yellow solid (yield 93%). ^{1}H NMR (400 MHz, DMSO-d_6): δ 7.96 (d, J = 2.5 Hz, 1H), 7.60 (d, J = 2.6 Hz, 1H), 6.37 (s, 2H), 0.24 (s, 9H). MS (ESI) m/z: 225.2 [M + H]$^+$.

*6-Amino-5-((trimethylsilyl)ethynyl)nicotinamide (**39f**).* It is obtained as a gray solid (yield 76%). ^{1}H NMR (400 MHz, DMSO-d_6): δ 8.48 (d, J = 2.3 Hz, 1H), 7.99 (d, J = 2.3 Hz, 1H), 7.76 (s, 1H), 7.16 (s, 1H), 6.70 (s, 2H), 0.24 (s, 9H). MS (ESI) m/z: 234.2 [M + H]$^+$.

*6-Amino-N-methyl-5-((trimethylsilyl)ethynyl)nicotinamide (**39g**).* It is obtained as a yellow solid (92%). ^{1}H NMR (400 MHz, Chloroform-d): δ 8.43 (d, J = 1.9 Hz, 1H), 7.94 (d, J = 1.8 Hz, 1H), 6.12 (br s, 1H), 5.42 (s, 2H), 2.96 (d, J = 4.7 Hz, 3H), 0.25 (s, 9H). MS (ESI) m/z: 248.1 [M + H]$^+$.

*Methyl 6-Amino-5-((trimethylsilyl)ethynyl)nicotinate (**39h**).* It is obtained as a black solid (yield 78%). ^{1}H NMR (400 MHz, DMSO-d_6): δ 8.52 (s, 1H), 7.88 (d, J = 2.0 Hz, 1H), 7.06 (s, 2H), 3.77 (s, 3H), 0.24 (s, 8H). MS (ESI) m/z: 249.5 [M + H]$^+$.

*5-Bromo-3-((trimethylsilyl)ethynyl)pyridin-2-amine (**39i**).* It is obtained as a yellow solid (yield 82.6%). ^{1}H NMR (400 MHz, DMSO-d_6): δ 8.02 (d, J = 2.4 Hz, 1H), 7.69 (d, J = 2.5 Hz, 1H), 6.37 (s, 2H), 0.24 (s, 9H). MS (ESI) m/z: 269.2 [M + H]$^+$.

*3-Iodo-4-isopropylbenzoic acid (**40c**).* Step 1: To a solution of 4-isopropylbenzoic acid (5.0 g, 30.45 mmol) in DMF (60 mL) were added K_2CO_3 (12.62 g, 91.35 mmol) and MeI (482 μL, 36.54 mmol) at rt, and the mixture was stirred at this temperature for 2 h. After being cooled down to 0 °C, saturated aqueous (sat. aq) $Na_2S_2O_3$ solution (10 mL) was poured into the resulting solution and stirred at rt for 20 min. The mixture was poured into water and extracted with EtOAc. The organic layer was washed with water and brine, dried with Na_2SO_4, filtered, and concentrated under reduced pressure to give methyl 4-isopropylbenzoate as light yellow oil (5.4 g, yield 99%). The crude product was used directly for the next step without further purification. Step 2: To a solution of methyl 4-isopropylbenzoate (4.2 g, 23.60 mmol) in AcOH/Ac_2O (30 mL, 2:1, v/v) were added $NaIO_4$ (2.6 g, 12.11 mmol) and I_2 (2.0 g, 8.01 mmol) at 0 °C. Concentrated H_2SO_4 (10 mL, 184 mmol) was added dropwise into the solution, and the mixture was stirred at 40 °C for 4 h. Water (40 mL) and sat. aq $Na_2S_2O_3$ solution (25 mL) was added into the resulting solution under an ice bath. After stirring at rt for 30 min, the mixture was extracted with CH_2Cl_2. The organic layer was washed with water and brine and dried with Na_2SO_4. The resultant crude material was purified by flash column chromatography (SiO_2, petroleum ether/EtOAc, 50:1) to give methyl 3-iodo-4-isopropylbenzoate as yellow oil (5.1 g, yield 71.16%). Step 3: To a solution of methyl 3-iodo-4-isopropylbenzoate (3.1 g, 10.19 mmol) in THF/MeOH/H_2O (35 mL, 4:1:1, v/v/v) was added LiOH·H_2O (1.1 g, 26.21 mmol) at rt, and the mixture was stirred for 5 h. The resulting solution was cooled down in an ice bath, then the pH was adjusted to 4−5 with diluted hydrochloric acid (1 M), and the product was precipitated. After stirring at 0 °C for 30 min, the mixture was filtrated. The filter cake was rinsed with water (3 × 15 mL) and then dried in a vacuum oven

https://dx.doi.org/10.1021/acs.jmedchem.9b01912
J. Med. Chem. XXXX, XXX, XXX−XXX

to give **40c** as a yellow solid (2.8 g, yield 95%). ^{1}H NMR (400 MHz, DMSO-d_6): δ 12.99 (s, 1H), 8.32 (s, 1H), 7.91 (d, J = 8.1 Hz, 1H), 7.45 (d, J = 8.1 Hz, 1H), 3.24 (hept, J = 6.8 Hz, 1H), 1.19 (d, J = 6.7 Hz, 6H). MS (ESI) m/z: 290.3 $[M + H]^+$.

*N-(3,5-Dimethoxyphenyl)-3-iodo-4-methylbenzamide (**41a**).* It is obtained as a yellow solid (2.5 g, yield 82%). ^{1}H NMR (400 MHz, DMSO-d_6): δ 10.17 (s, 1H), 8.38 (d, J = 1.9 Hz, 1H), 7.88 (dd, J = 1.9, 7.9 Hz, 1H), 7.48 (d, J = 8.2 Hz, 1H), 7.07 (d, J = 2.3 Hz, 2H), 6.27 (t, J = 2.3 Hz, 1H), 3.73 (s, 6H). MS (ESI) m/z: 398.2 $[M + H]^+$.

*N-(3,5-Dimethoxyphenyl)-3-iodobenzamide (**41b**).* It is obtained as a yellow solid (yield 90%). ^{1}H NMR (400 MHz, methanol-d_4): δ 8.24 (d, J = 15.2 Hz, 1H), 7.91 (t, J = 8.0 Hz, 2H), 7.28 (t, J = 7.8 Hz, 1H), 6.96 (s, 2H), 6.29 (s, 1H), 3.78 (s, 6H). MS (ESI) m/z: 384.1 $[M + H]^+$.

*N-(3,5-Dimethoxyphenyl)-3-iodo-4-isopropylbenzamide (**41c**).* It is obtained as a yellow solid (yield 85%). ^{1}H NMR (400 MHz, DMSO-d_6): δ 9.09 (s, 1H), 8.33 (d, J = 2.9 Hz, 1H), 7.88 (dd, J = 15.0, 3.1 Hz, 1H), 7.33 (d, J = 15.0 Hz, 1H), 7.01 (d, J = 3.1 Hz, 2H), 6.23 (t, J = 3.0 Hz, 1H), 3.79 (s, 6H), 3.04−2.69 (m, 1H), 1.17 (d, J = 12.7 Hz, 6H). MS (ESI) m/z: 426.1 $[M + H]^+$.

*N-(3,5-Dimethoxyphenyl)-3-iodo-4-methoxybenzamide (**41d**).* It is obtained as a gray solid (yield 84%). ^{1}H NMR (400 MHz, methanol-d_4): δ 8.37 (s, 1H), 7.97 (d, J = 8.9 Hz, 1H), 7.05 (d, J = 8.7 Hz, 1H), 6.96 (s, 2H), 6.29 (s, 1H), 3.95 (s, 3H), 3.78 (s, 6H). MS (ESI) m/z: 414.1 $[M + H]^+$.

*3-Bromo-N-(3,5-dimethoxyphenyl)-4-fluorobenzamide (**41e**).* It is obtained as a gray solid (yield 76%). ^{1}H NMR (400 MHz, DMSO-d_6): δ 10.27 (s, 1H), 8.30 (d, J = 6.1 Hz, 1H), 8.02 (m, 1H), 7.54 (m, 1H), 7.06 (s, 2H), 6.28 (s, 1H), 3.74 (s, 6H). MS (ESI) m/z: 402.1 $[M + H]^+$.

*4-Chloro-N-(3,5-dimethoxyphenyl)-3-iodobenzamide (**41f**).* It is obtained as a white solid (yield 86%). ^{1}H NMR (400 MHz, methanol-d_4): δ 8.43 (s, 1H), 7.88 (d, J = 8.2 Hz, 1H), 7.60 (d, J = 8.3 Hz, 1H), 6.95 (s, 2H), 6.28 (s, 1H), 3.77 (s, 6H). MS (ESI) m/z: 418.2 $[M + H]^+$.

*3-Bromo-N-(3,5-dimethoxyphenyl)-4-(trifluoromethyl)-benzamide (**41g**).* It is obtained as a white solid (yield 77.8%). ^{1}H NMR (400 MHz, methanol-d_4): δ 8.32 (s, 1H), 8.03 (d, J = 7.9 Hz, 1H), 7.91 (d, J = 8.0 Hz, 1H), 6.98 (s, 2H), 6.32 (s, 1H), 3.79 (s, 6H). MS (ESI) m/z: 452.1 $[M + H]^+$.

*5-((2-Amino-5-bromopyridin-3-yl)ethynyl)-N-(3,5-dimethoxyphenyl)-2-methylbenz-amide (**42a**).* It is obtained as a yellow solid (yield 81%). ^{1}H NMR (400 MHz, DMSO-d_6): δ 10.20 (s, 1H), 8.25 (s, 1H), 8.06 (d, J = 2.3 Hz, 1H), 7.86 (d, J = 5.1 Hz, 1H), 7.85 (s, 1H), 7.47 (d, J = 8.1 Hz, 1H), 7.09 (d, J = 1.9 Hz, 2H), 6.62 (s, 2H), 6.27 (s, 1H), 3.74 (s, 6H), 2.54 (s, 3H). MS (ESI) m/z: 467.3 $[M + H]^+$.

*3-((2-Amino-5-bromopyridin-3-yl)ethynyl)-N-(3,5-dimethoxyphenyl)benzamide (**42b**).* It is obtained as a yellow solid (yield 79.6%). ^{1}H NMR (400 MHz, DMSO-d_6): δ 10.29 (s, 1H), 8.22 (s, 1H), 8.05 (s, 1H), 7.93 (d, J = 7.2 Hz, 1H), 7.86 (d, J = 8.0 Hz, 1H), 7.82 (br s, 1H), 7.59 (t, J = 7.7 Hz, 1H), 7.09 (s, 2H), 6.71 (s, 2H), 6.28 (s, 1H), 3.74 (s, 6H). MS (ESI) m/z: 453.1 $[M + H]^+$.

*3-((2-Amino-5-bromopyridin-3-yl)ethynyl)-N-(3,5-dimethoxyphenyl)-4-isopropylbenzamide (**42c**).* It is obtained as a yellow solid (yield 79%). ^{1}H NMR (400 MHz, DMSO-d_6): δ 10.23 (s, 1H), 8.31−8.24 (m, 2H), 8.09 (s, 1H), 7.92 (d, J = 8.2 Hz, 1H), 7.85 (s, 1H), 7.55 (m, 1H), 7.12 (d, J = 2.2 Hz, 2H), 6.31 (s, 1H), 6.28 (t, J = 2.1 Hz, 1H), 3.74 (s, 6H), 3.57 (m, J = 13.7, 6.9 Hz, 1H), 1.29 (d, J = 6.8 Hz, 6H). MS (ESI) m/z: 495.1 $[M + H]^+$.

*3-((2-Amino-5-bromopyridin-3-yl)ethynyl)-N-(3,5-dimethoxyphenyl)-4-methoxybenzamide (**42d**).* It is obtained as a yellow solid (yield 77%). ^{1}H NMR (400 MHz, DMSO-d_6): δ 10.13 (s, 1H), 8.22 (s, 1H), 8.07 (d, J = 2.4 Hz, 1H), 8.01 (d, J = 8.6 Hz, 1H), 7.77 (d, J = 2.3 Hz, 1H), 7.62 (s, 1H), 7.26 (d, J = 8.7 Hz, 1H), 7.08 (d, J = 2.1 Hz, 2H), 6.58 (s, 1H), 6.26 (s, 1H), 3.97 (s, 3H), 3.74 (s, 6H). MS (ESI) m/z: 483.3 $[M + H]^+$.

*3-((2-Amino-5-bromopyridin-3-yl)ethynyl)-N-(3,5-dimethoxyphenyl)-4-fluorobenzamide (**42e**).* *General Procedure for Syntheses of **42e−f**.* To a solution of **41e** (200 mg, 0.56 mmol) in dry MeCN (40 mL) were added **39i** (205 mg, 0.76 mmol), CsF (214 mg, 1.41 mmol), and Et_3N (235 μL, 1.69 mmol) at rt under a N_2 atmosphere. The mixture was heated to 80 °C and stirred for 4 h. The resulting solution was poured into water and extracted with EtOAc. The organic layer was washed with brine and dried with Na_2SO_4. The crude material was purified by flash column chromatography (SiO_2, CH_2Cl_2/MeOH, 25:1) to give **42e** as a yellow solid (220 mg, yield 82.8%). ^{1}H NMR (400 MHz, DMSO-d_6): δ 10.29 (s, 1H), 8.39 (d, J = 5.8 Hz, 1H), 8.11−8.06 (m, 1H), 8.04−7.97 (m, 1H), 7.83 (dd, J = 9.3, 1.9 Hz, 1H), 7.51 (t, J = 9.0 Hz, 1H), 7.07 (br s, 2H), 6.78 (s, 1H), 6.70 (s, 2H), 6.28 (s, 1H), 3.74 (s, 6H). MS (ESI) m/z: 470.2 $[M + H]^+$.

*3-((2-Amino-5-bromopyridin-3-yl)ethynyl)-4-chloro-N-(3,5-dimethoxyphenyl)benzamide (**42f**).* It is obtained as a yellow solid (yield 76%). ^{1}H NMR (400 MHz, DMSO-d_6): δ 10.34 (s, 1H), 8.40 (d, J = 2.2 Hz, 1H), 8.10 (d, J = 2.5 Hz, 1H), 7.94 (dd, J = 8.5, 2.2 Hz, 1H), 7.83 (d, J = 2.4 Hz, 1H), 7.77 (d, J = 8.4 Hz, 1H), 7.65−7.54 (m, 2H), 7.07 (d, J = 2.2 Hz, 2H), 6.29 (t, J = 2.2 Hz, 1H), 3.74 (s, 6H). MS (ESI) m/z: 487.1 $[M + H]^+$.

*3-((2-Amino-5-bromopyridin-3-yl)ethynyl)-N-(3,5-dimethoxyphenyl)-4-(trifluoromethyl)benzamide (**42g**).* It is obtained as a yellow solid (yield 60%). ^{1}H NMR (400 MHz, methanol-d_4): δ 8.34 (s, 1H), 8.06 (s, 2H), 7.92 (d, J = 8.5 Hz, 1H), 7.77 (s, 1H), 7.00 (s, 2H), 6.33 (s, 1H), 5.50 (s, 1H), 3.80 (s, 6H). MS (ESI) m/z: 520.1 $[M + H]^+$.

*Methyl 3-((2-Amino-5-(1-methyl-1H-pyrazol-4-yl)pyridin-3-yl)-ethynyl)-4-methylbenzoate (**44**).* Step 1: To a solution of **43** (5.0 g, 18.11 mmol) in dry MeCN (150 mL) were added **39i** (6.3 g, 23.54 mmol), $Pd(PPh_3)_2Cl_2$ (636 mg, 0.91 mmol), CuI (345 mg, 1.81 mmol), CsF (6.9 g, 45.28 mmol), and Et_3N (7.6 mL, 54.3 mmol) at rt under a N_2 atmosphere, and the mixture was stirred for 6 h. The resulting solution was filtered through a pad of Celite, and the solvent was removed by reduced pressure. The resultant crude material was purified by flash column chromatography (SiO_2, petroleum ether/EtOAc, 8:1) to give methyl 3-((2-amino-5-bromopyridin-3-yl)-ethynyl)-4-methylbenzoate (yellow solid, 6.0 g, yield 96%). The product obtained above (6.0 g, 17.38 mmol) was dissolved in THF/H_2O (150 mL, 4:1, v/v), followed by the addition of 1-methyl-4-(4,4,5,5-tetramethyl-1,3,2-dioxaborolan-2-yl)-1*H*-pyrazole (5.4 g, 26.07 mmol), $Pd(OAc)_2$ (0.4 g, 1.74 mmol), X-Phos (1.7 g, 3.48 mmol), and K_2CO_3 (6.0 g, 43.45 mmol) under a N_2 atmosphere. The mixture was refluxed at 90 °C for 6 h. The resulting solution was filtered through a pad of Celite, and the filtrate was removed by reduced pressure to give the crude material, which was further purified by flash column chromatography (SiO_2, petroleum ether/EtOAc, 2:1) to give **44** as a yellow solid (5.9 g, yield 98%). ^{1}H NMR (400 MHz, DMSO-d_6): δ 8.28−8.23 (m, 2H), 8.08 (s, 1H), 7.88−7.84 (m, 3H), 7.82 (s, 1H), 7.48 (d, J = 8.0 Hz, 1H), 6.35 (s, 2H), 3.87 (s, 3H), 3.84 (s, 3H), 2.56 (s, 3H). MS (ESI) m/z: 347.2 $[M + H]^+$.

*3-((2-Amino-5-(1-methyl-1H-pyrazol-4-yl)pyridin-3-yl)ethynyl)-4-methylbenzoic acid (**45**).* To a solution of **44** (5.9 g, 17.03 mmol) in THF/MeOH/H_2O (90 mL, 4/1/1, v/v/v) was added LiOH·H_2O (1.8 g, 42.58 mmol) at rt, and the mixture was stirred at this temperature for 12 h. The resulting solution was cooled to 0 °C, and then the pH was adjusted to 4−5 with diluted hydrochloric acid (1 M), and the product was precipitated. After stirring for 30 min at 0 °C, the mixture was filtered, and the filter cake was rinsed with water (3 × 15 mL) and then dried in a vacuum oven to give **45** as a yellow-green solid (5.2 g, yield 92%). ^{1}H NMR (400 MHz, DMSO-d_6): δ 13.06 (br s, 1H), 8.26 (s, 1H), 8.22 (s, 1H), 8.08 (s, 1H), 7.88−7.80 (m, 3H), 7.45 (d, J = 8.0 Hz, 1H), 6.35 (s, 2H), 3.84 (s, 3H), 2.55 (s, 3H). MS (ESI) m/z: 333.2 $[M + H]^+$.

*N-(4-Chlorophenyl)-4-iodo-3-methylbenzamide (**48a**).* It is obtained as a light pink solid (yield 90%). ^{1}H NMR (400 MHz, chloroform-d): δ 7.92 (d, J = 8.3 Hz, 1H), 7.81 (s, 1H), 7.71 (s, 1H), 7.58 (d, J = 8.6 Hz, 2H), 7.33 (d, J = 8.4 Hz, 2H), 2.50 (s, 3H). MS (ESI) m/z: 371.2 $[M + H]^+$.

https://dx.doi.org/10.1021/acs.jmedchem.9b01912
J. Med. Chem. XXXX, XXX, XXX−XXX

*4-Chloro-N-(3-iodo-4-methylphenyl)benzamide (**48b**).* It is obtained as a white solid (yield 88%). ^{1}H NMR (400 MHz, DMSO-d_6): δ 10.32 (s, 1H), 8.31 (d, J = 2.1 Hz, 1H), 8.07−7.89 (m, 2H), 7.70 (dd, J = 8.3, 2.1 Hz, 1H), 7.68−7.56 (m, 2H), 7.30 (d, J = 8.5 Hz, 1H), 2.34 (s, 3H). MS (ESI) m/z: 371.2 $[M + H]^+$.

*N-(4-Chlorophenyl)-3-iodo-4-methylbenzamide (**48c**).* It is obtained as a white solid (yield 79%). ^{1}H NMR (400 MHz, DMSO-d_6): δ 10.38 (s, 1H), 8.39 (d, J = 1.8 Hz, 1H), 7.89 (dd, J = 7.9, 1.9 Hz, 1H), 7.82 (d, J = 8.9 Hz, 2H), 7.47 (d, J = 7.7 Hz, 1H), 7.41 (d, J = 8.8 Hz, 2H), 2.44 (s, 3H). MS (ESI) m/z: 371.2 $[M + H]^+$.

*N-(4-Chlorophenyl)-3-iodo-N,4-dimethylbenzamide (**49**).* A solution of **48c** (1.0 g, 2.69 mmol) in anhydrous THF (25 mL) was added dropwise to a suspension of NaH (60%, 215 mg, 5.38 mmol) in anhydrous THF (20 mL) under stirring at 0 °C. After stirring at 0 °C for 15 min, MeI (335 μL, 5.38 mmol) was added to the reaction solution. The resulting solution was stirred at rt for 5 h and then cooled in an ice bath. After addition of water, the aqueous layer was extracted with CH_2Cl_2. The combined organic layers were washed with sat. aq $Na_2S_2O_3$ solution and brine and dried with Na_2SO_4. The crude product was purified by flash chromatography (SiO_2, petroleum ether/EtOAc, 5:1) to give **49** as a light yellow solid (890 mg, 86%). ^{1}H NMR (400 MHz, DMSO-d_6): δ 7.72 (d, J = 1.4 Hz, 1H), 7.34 (d, J = 8.8 Hz, 2H), 7.22 (d, J = 8.7 Hz, 2H), 7.16 (d, J = 7.9 Hz, 1H), 7.11 (dd, J = 7.9, 1.4 Hz, 1H), 3.32 (s, 3H), 2.27 (s, 3H). MS (ESI) m/z: 385.1 $[M + H]^+$.

*4-Chloro-N-(3-iodo-4-methylbenzyl)aniline (**50**).* To a solution of **48c** (1.0 g, 2.69 mmol) in anhydrous THF (20 mL) was added 1.0 M BH_3·THF (5.4 mL) solution dropwise at rt, and the reaction mixture was stirred at this temperature for 12 h. The resulting solution was diluted with EtOAc (20 mL) and quenched by the careful addition of sat. aq $NaHCO_3$ solution (5 mL). The organic layer was washed with sat. aq sodium potassium tartrate solution (30 mL), 10% aq. Na_2CO_3 solution (30 mL), and brine (30 mL), dried with anhydrous Na_2SO_4, filtered, and concentrated under reduced pressure. The resulting crude product was purified by flash column chromatography (SiO_2, petroleum ether/EtOAc, 10:1) to give **50** as a white solid (427 mg, yield 44%). ^{1}H NMR (400 MHz, chloroform-d): δ 7.90 (s, 1H), 7.35−7.28 (m, 2H), 7.21 (d, J = 8.9 Hz, 2H), 6.63 (d, J = 8.9 Hz, 2H), 4.33 (s, 2H), 4.15 (br s, 1H), 2.52 (s, 3H). MS (ESI) m/z: 357.3 $[M + H]^+$.

Reagents and Antibodies. Compound PLX3397 (batch number: 160823; purity: 98%) was purchased from Yi shiming (Beijing) biological medicine technology co. LTD. Compounds were dissolved in dimethyl sulfoxide (DMSO, Sigma-Aldrich) at a concentration of 50 mmol/L and then diluted with the Dulbecco's modified Eagle's medium (DMEM) medium (Hyclone, South Logan, UT, USA) containing 10% fetal bovine serum (FBS, Hyclone). CCK-8 was purchased from Dojindo (Kumamoto, Japan). LPS was purchased from Sigma (St Louis, MO, USA). Primary antibodies against CSF1R (3152), phosphor-CSF1R (Tyr723, 3151), Akt (9272), and phosphor-Akt (Ser473, 4060) were purchased were purchased from Cell Signaling Technology (CST, Boston, MA, USA). Actin was purchased from Abgent (Abgent, San Diego, CA, USA), and anti-rabbit IgG horseradish peroxidase (HRP)-linked secondary antibody was purchased from Bio-Rad (Bio-Rad, Hercules, CA, USA).

Cell Lines. The murine macrophage RAW 264.7 cells (ATCC, Manassas, VA, USA) were cultured in DMEM containing 10% fetal bovine serum (FBS), 2 mmol/L of L-glutamine, 100 U/mL penicillin, and 100 μg/mL streptomycin. The cells were maintained at 37 °C in a 5% CO_2 incubator.

In Vitro Kinase Enzyme Assay. The kinase inhibitory activity of each compound was determined using an enzyme-linked immunosorbent assay (ELISA). Recombinant proteins, including CSF1R, VEGFRs, PDGFRs, EGFRs, RET, c-Kit, Flt3, Src, Abl, EphA2, IGF1R, IR, FGFRs, BTK, FAK, ITK, and ACK1, were purchased from Millipore (UK, LTD). Briefly, the 96-well ELISA plates were precoated with substrate poly (Glu, Tyr)$_{4:1}$ (Sigma, St. Louis, MO, USA). Active kinases were added into the plate and incubated with the compound in reaction buffer containing 5 μM ATP. After incubation at 37 °C for 1 h, the wells were washed and incubated with PY99 antibody (Santa Cruz Biotechnology, Santa Cruz, CA), followed by a HRP-conjugated secondary antibody. The wells were visualized using *o*-phenylenediamine and read with a multiwell spectrophotometer (SpectraMax Plus384, Molecular Devices) at an absorbance of 490 nM.

Cell Viability Assay. The cytotoxicity of the compounds was evaluated by the CCK-8. Briefly, the cells (5×10^4 cells/well) were seeded into 96-well plates in triplicate with 200 μL of DMEM media for 24 h in the presence or absence of indicated concentrations of compounds. Subsequently, a total of 20 μL CCK-8 was added to each well. After 1 h incubation, the plates were measured at 450 nm (570 nm calibration) using a microplate reader (Molecular Devices, Sunnyvale, CA, USA), and the cell viability was calculated. The cytotoxicity of the compounds was expressed as CC_{50}, using the log (inhibitor) versus normalized response nonlinear fit (GraphPad Prism 8.0).

Western Blot Assay. RAW264.7 cells (1×10^6 cells/well) were seeded into six-well plates and incubated overnight and then treated with or without different concentrations of compound **29** for 6 h and then stimulated with or without CSF-1 (100 ng/mL) for 20 min. Cell samples were then lysed in 1× SDS lysis buffer (Beyotime, Shanghai, China) and uniformed by the Pierce BCA protein assay kit (Thermo Fisher Scientific, Pittsburgh, PA, USA). Equal protein amounts were loaded to 10% sodium dodecyl sulfate polyacrylamide gel electrophoresis and transferred to a nitrocellulose membrane (Bio-Rad, Hercules, CA, USA), which was blocked with SuperBlockTM T20 blocking buffer (Thermo Fisher Scientific, Pittsburgh, PA, USA) and then incubated overnight at 4 °C with primary antibodies. The bands were incubated with HRP-conjugated anti-rabbit IgG (Bio-Rad, Richmond, CA, USA) and further visualized using a SuperSignalTM West Femto Maximum Sensitivity Substrate kit (Thermo Fisher Scientific, Pittsburgh, PA, USA) under the ChemiDocTM MP Imaging System (Bio-Rad, Richmond, CA, USA).

In Vitro Anti-Inflammatory Activity Assay. RAW264.7 cells were incubated with compounds or the media (0.125% DMSO in DMEM containing 10% FBS), and then the cells were primed with LPS (1 μg/mL) for 24 h. The supernatants were collected and then measured using the mouse TNF-α and IL-6 ELISA kit. The IC_{50} values were estimated using the log (inhibitor) versus normalized response nonlinear fit (Graph Pad Prism 8.0).

Determination of PK Parameters in Rats. Male SD rats (200 ± 20 g) were purchased from B&K Universal Group Co. Ltd. (Shanghai, China). All the animal studies were performed according to the protocols and guidelines of the Institutional Care and Use Committee of the Shanghai Institute of Materia Medica. Rats were housed in a well-lit air-conditioned animal room at 19−23 °C with 50−60% relative humidity under standard environmental conditions (12 h light/dark cycle). Rats were fed with standard rodent chow and water at libitum. After acclimation to the laboratory for at least 1 week, rats were randomly divided into two groups (each group 3) and then fasted for 12 h with free access to water prior to the experiment. One group was injected with intravenously (iv) formulation at doses of 2 mg/kg compound **29**, and the other group was treated by oral gavage (p.o.) of p.o. formulation at doses of 5 mg/kg compound **29**. The p.o. formulation was prepared with DMSO/HPMC (5/95, v/v). The iv formulation was made with DMSO/EtOH/PEG300/Saline (5/5/40/50, v/v/v/v). Blood samples (40 μL) from the femoral vein were collected into a heparinized tube at 15, 30, 60, 120, 240, 480, and 1440 min after administration. Blood samples were immediately centrifuged at 4 °C and 12 000*g* for 5 min to obtain plasma, which was then transferred to a clean vial and subsequently stored at −20 °C until analysis. The plasma sample (20 μL) was precipitated with 200 μL of methanol containing the geniposide (IS) (20 ng/mL) and vigorously vortex-mixed for 1 min. After centrifugation at 12 000*g* for 5 min at 4 °C, the supernatants from each sample were analyzed using LC−MS/MS with an Acquity ultra performance liquid chromatography system (I-class, Waters, Milford, USA) coupled to a triple quadrupole mass spectrometer (Xevo TQ-S, Waters, Milford, USA).

The chromatographic separation was performed on a Welch Xtimate C18 column (50 × 2.1 mm, 1.7 μm) at a low flow rate (0.35

https://dx.doi.org/10.1021/acs.jmedchem.9b01912
J. Med. Chem. XXXX, XXX, XXX−XXX

mL/min). Plasma amples or calibration standards (5 μL) were injected into the system, and the temperature of column and autosampler was maintained at 45 and 10 °C, respectively. Mobile phases: A, H_2O (5 mM ammonium acetate and 0.1% HCOOH); B, MeCN (0.1% HCOOH). The gradient program was listed as follow: 0.0−0.1 min, 10% (v/v) B; 0.1−0.8 min, 10−95% B; 0.8−1.8 min, 95% B; 1.8−1.81 min, 95−10% B; 1.81−3.0 min, and 10% B. The mass spectrometer equipped with an electrospray ionization probe was operated in a positive ion mode with a capillary voltage 3.0 kV at a temperature of 500 °C, and the desolvation gas flow 1000 L/h. Quantitative analysis was performed by monitoring $[M + H]^+$ for the compound **29** and IS in multiple reaction monitoring modes. PK parameters were calculated using a noncompartmental model of Phoenix 1.3 software (US Pharsight Corporation). The peak concentration C_{max} and the peak time T_{max} were measured; the area under the concentration time curve of AUC_{0-t} value was calculated by the trapezoidal method; $AUC_{0-\infty} = AUC_{0-t} + C_t/k_e$, where C_t is the last blood concentration that can be measured, k_e is the elimination rate constant; elimination half-life $t_{1/2} = 0.693/k_e$; mean residence time MRT = AUMC/AUC; clearance CL = $D/AUC_{0-\infty}$; steady-state distribution volume V_{ss} = CL × MRT; absolute bioavailability $F = AUC_{0-\infty}(oral)/AUC_{0-\infty}(i.v.) \times dose(i.v.)/dose(oral) \times 100\%$.

In Vivo Anti-Inflammatory Efficacy Investigation. All the animal studies were performed according to the protocols and guidelines of the institutional care and use committee. Inbred 8-week-old female BALB/c mice were purchased from Shanghai Lingchang Biotechnology Co., Ltd. (Certificate no. 2013-0018, Shanghai, China). All mice were housed under specific pathogen-free conditions and raised in a 12 h light/dark cycle with humidity (60−80%) and temperature (22 ± 1 °C). All mice were fed standard laboratory chow and water at libitum and allowed to acclimatize in our facility for 1 week before any experiments started. Mice were randomly divided into five groups with six mice per group: untreated normal control, vehicle (0.5% sodium carboxymethylcellulose and 0.25% Tween-80), PLX3397 (40 mg/kg), and compound **29** (20 and 40 mg/kg). Vehicle, PLX3397, and compound **29** were orally administrated at 4 h before intraperitoneal injection with a dose of 5 mg/kg of LPS. Blood sample (0.1 mL) was collected via orbital sinus puncture at 1.5 and 3 h after LPS application. The blood sample was centrifuged at 4 °C and 12 000 rpm for 10 min, and then the serum was transferred to a clean tube and stored at −80 °C prior to analysis. The serum of each mouse from all groups was determined by using mouse IL-6 and TNF-α ELISA kits, according to the manufacturer instructions. All ELISA quantification kits were purchased from BD Pharmingen (San Diego, CA, USA).

Molecular Modeling. Ligands were created with ChmBio3D Ultra 14.0 and minimized according to the MMFF94 force field. Molecular docking of compounds (**7**, **8**, **12**, **16**, and **29**) into CSF-1R (PDB code: 4R7H and 4R7I) and FGFR1 (PDB code: 4V04) kinases was performed in AutoDock Vina.[23] For preparation of the macromolecule and ligands, water was excluded, and Gasteiger charges were assigned for the protein. Torsional root and the rotatable bonds of the ligand were identified. Prior to the AutoDock, AutoGrid was carried out for the preparation of the grid map using a grid box, which was centered at the original ligand and extended outward the ligand within the 5 Å domain. A scoring grid was calculated from the original ligand structure to minimize the computation time. Finally, AutoDock vina was performed using the Lamarckian Genetic Algorithm with default settings, and the top ranked poses were visually inspected. The docking results were shown as the cartoon model in Pymol.

Statistical Analysis. All experiment data were presented as mean ± SEM and statistically evaluated by one-way ANOVA followed by Dunnett's test between different groups. Statistical analyses were evaluated using GraphPad Prism 8.0 software. Differences where $p < 0.05$ were considered statistically significant.

■ ASSOCIATED CONTENT

Supporting Information

The Supporting Information is available free of charge at https://pubs.acs.org/doi/10.1021/acs.jmedchem.9b01912.

Blockade effect of **29** on the hERG channel, ^1H NMR, ^{13}C NMR spectra of compounds **7**−**37**, and ^{19}F NMR spectra of **7**, **20**, **22**, **30**, and **31**, and the purity data of all final compounds (PDF)

Molecular formula strings and some data (CSV)

Accession Codes

PDB code 4R7H was used for modeling docking of compound **7**, **8**, **12**, **16**, and **29** in CSF-1R; PDB code 4R7I was used for modeling docking of compound **7** and **8**; PDB code 4V04 was used for modeling docking of compound **7** and **8** in FGFR1.

■ AUTHOR INFORMATION

Corresponding Authors

Hua Xie − *Chinese Academy of Sciences, Shanghai, China, and University of Chinese Academy of Sciences, Beijing, China*; Email: hxie@simm.ac.cn

Wei Tang − *Chinese Academy of Sciences, Shanghai, China, and University of Chinese Academy of Sciences, Beijing, China*; Email: tangwei@simm.ac.cn

Youhong Hu − *Chinese Academy of Sciences, Shanghai, China, and University of Chinese Academy of Sciences, Beijing, China*; orcid.org/0000-0003-1770-6272; Phone: +86-21-50806600-3526; Email: yhhu@simm.ac.cn

Other Authors

Zhicheng Xie − *Chinese Academy of Sciences, Shanghai, China, and University of Chinese Academy of Sciences, Beijing, China*

Bing Wu − *Chinese Academy of Sciences, Shanghai, China, and University of Chinese Academy of Sciences, Beijing, China*

Yingqiang Liu − *Chinese Academy of Sciences, Shanghai, China, and Fudan University, Shanghai, China*

Wenming Ren − *Chinese Academy of Sciences, Shanghai, China*

Linjiang Tong − *Chinese Academy of Sciences, Shanghai, China, and University of Chinese Academy of Sciences, Beijing, China*

Caigui Xiang − *Chinese Academy of Sciences, Shanghai, China, and University of Chinese Academy of Sciences, Beijing, China*

Aihuan Wei − *Chinese Academy of Sciences, Shanghai, China*

Yuanzhuo Gao − *Chinese Academy of Sciences, Shanghai, China, and University of Chinese Academy of Sciences, Beijing, China*

Limin Zeng − *Chinese Academy of Sciences, Shanghai, China*

Complete contact information is available at: https://pubs.acs.org/10.1021/acs.jmedchem.9b01912

Author Contributions

⊥Z.X., B.W., and Y.L. contributed equally to this work.

https://dx.doi.org/10.1021/acs.jmedchem.9b01912
J. Med. Chem. XXXX, XXX, XXX−XXX

Notes

The authors declare no competing financial interest.

■ ACKNOWLEDGMENTS

This study was financially supported by the National Science and Technology Major Project Key New Drug Creation and Manufacturing of China (2018ZX09711002), Science and Technology Commission of Shanghai Municipality (18431907100), and the State Key Laboratory of Drug Research (SIMM1803ZZ-01).

■ ABBREVIATIONS

CSF-1R, colony stimulating factor 1 receptor kinase; HTS, high-throughput screening; FLT-3, FMS-like tyrosine kinase 3; KIT, stem cell factor receptor; PDGFR, platelet-derived growth factor receptor; TNF-α, tumor necrosis factor-α; IL-6, interleukin-6; RA, rheumatoid arthritis; AD, Alzheimer's disease; PVNS/dt-GCT, pigmented villonodular synovitis; FGFR, fibroblast growth factor receptor; DFG, asparticacid-phenylalanine-glycine; PDB, Protein Data Bank; Phe, phenylalanine; Ile, isoleucine; HishistidineCys, histidineCyscysteine; Trp, tryptophan; Glu, glutamicacid; Asp, asparticacid; JM, juxtamembrane; Gly, glycine; Tyr, tyrosine; Val, valine; Ala, alanine; Lys, lysine; Thr, threonine; SAR, structure−activity relationship; IC_{50}, half maximal (50%) inhibitory concentration (IC); Het., aromatic heterocycle; HD, hydrogen bond donor; EGFR, epidermal growth factor receptor; ErbB2/4, human epidermal growth factor receptor 2/4; VEGFR, vascular endothelial growth factor receptor; IGF1R, insulin-like growth factor 1-receptor; IR, insulin receptor; RET, proto-oncogene tyrosine-protein kinase receptor Ret; BTK, Bruton's tyrosine kinase; Src, tyrosine kinases that encoded by the oncogenic retrovirus, Rous sarcoma virus; FAK, focal adhesion kinase; Abl, nonreceptor tyrosine kinase Abelson; ITK, IL2-inducible T-cell kinase; EphA2, ephrin type-A receptor 2; ACK1, activated CDC42 kinase 1; CC_{50}, median cytotoxic concentration; PK, PK; SD-rats, Sprague-Dawley rats; i.v., intravenous administration; p.o., oral gavage; AUC, the area under the concentration time curve; MRT, mean residence time; $t_{1/2}$, elimination half-life; T_{max}, the peak time; C_{max}, the peak concentration; CL, clearance; V_{ss}, steady-state distribution volume; F, absolute bioavailability; hERG, potassium-ion-channel; DMF, N,N-dimethylformamide; DIPEA, ethyldiisopropylamine; THF, tetrahydrofuran; TLC, thin-layer chromatography; UV, ultraviolet; ppm, parts per million

■ REFERENCES

(1) Sherr, C. J.; Rettenmier, C. W.; Roussel, M. F. Macrophage colony-stimulating factor, CSF1, and its proto-oncogene-encoded receptor. *Cold Spring Harbor Symp. Quant. Biol.* **1988**, *53*, 521−530.

(2) Woolford, J.; Rothwell, V.; Rohrschneider, L. Characterization of the human c-fms gene product and its expression in cells of the monocyte-macrophage lineage. *Mol. Cell. Biol.* **1985**, *5*, 3458−3466.

(3) Stanley, E. R.; Chitu, V. CSF-1 receptor signaling in myeloid cells. *Cold Spring Harbor Perspect. Biol.* **2014**, *6*, a021857.

(4) Bourette, R. P.; Rohrschneider, L. R. Early events in M-CSF receptor signaling. *Growth Factors* **2000**, *17*, 155−166.

(5) Kumari, A.; Silakari, O.; Singh, R. K. Recent advances in colony stimulating factor-1 receptor/c-FMS as an emerging target for various therapeutic implications. *Biomed. Pharmacother.* **2018**, *103*, 662−679.

(6) Chockalingam, S.; Ghosh, S. S. Macrophage colony-stimulating factor and cancer: a review. *Tumor Biol.* **2014**, *35*, 10635−10644.

(7) Huang, H.; Hutta, D. A.; Rinker, J. M.; Hu, H.; Parsons, W. H.; Schubert, C.; DesJarlais, R. L.; Crysler, C. S.; Chaikin, M. A.; Donatelli, R. R.; Chen, Y.; Cheng, D.; Zhou, Z.; Yurkow, E.; Manthey, C. L.; Player, M. R. Pyrido 2,3-d pyrimidin-5-ones: a novel class of antiinflammatory macrophage colony-stimulating factor-1 receptor inhibitors. *J. Med. Chem.* **2009**, *52*, 1081−1099.

(8) Illig, C. R.; Manthey, C. L.; Wall, M. J.; Meegalla, S. K.; Chen, J.; Wilson, K. J.; Ballentine, S. K.; DesJarlais, R. L.; Schubert, C.; Crysler, C. S.; Chen, Y.; Molloy, C. J.; Chaikin, M. A.; Donatelli, R. R.; Yurkow, E.; Zhou, Z.; Player, M. R.; Tomczuk, B. E. Optimization of a potent class of arylamide colony-stimulating factor-1 receptor inhibitors leading to anti-inflammatory clinical candidate 4-cyano-N-2-(1-cyclohexen-1-yl)-4- 1- (dimethylamino)acetyl -4-piperidi nyl phenyl -1H-imidazole-2-carboxamide (JNJ-28312141). *J. Med. Chem.* **2011**, *54*, 7860−7883.

(9) Zhang, C.; Ibrahim, P. N.; Zhang, J.; Burton, E. A.; Habets, G.; Zhang, Y.; Powell, B.; West, B. L.; Matusow, B.; Tsang, G.; Shellooe, R.; Carias, H.; Nguyen, H.; Marimuthu, A.; Zhang, K. Y. J.; Oh, A.; Bremer, R.; Hurt, C. R.; Artis, D. R.; Wu, G.; Nespi, M.; Spevak, W.; Lin, P.; Nolop, K.; Hirth, P.; Tesch, G. H.; Bollag, G. Design and pharmacology of a highly specific dual FMS and KIT kinase inhibitor. *Proc. Natl. Acad. Sci. U.S.A.* **2013**, *110*, 5689−5694.

(10) Martinez-Muriana, A.; Mancuso, R.; Francos-Quijorna, I.; Olmos-Alonso, A.; Osta, R.; Perry, V. H.; Navarro, X.; Gomez-Nicola, D.; Lopez-Vales, R. CSF1R blockade slows the progression of amyotrophic lateral sclerosis by reducing microgliosis and invasion of macrophages into peripheral Nerves. *Sci. Rep.* **2016**, *6*, 25663.

(11) Spangenberg, E.; Severson, P. L.; Hohsfield, L. A.; Crapser, J.; Zhang, J.; Burton, E. A.; Zhang, Y.; Spevak, W.; Lin, J.; Phan, N. Y.; Habets, G.; Rymar, A.; Tsang, G.; Walters, J.; Nespi, M.; Singh, P.; Broome, S.; Ibrahim, P.; Zhang, C.; Bollag, G.; West, B. L.; Green, K. N. Sustained microglial depletion with CSF1R inhibitor impairs parenchymal plaque development in an Alzheimer's disease model. *Nat. Commun.* **2019**, *10*, 3758.

(12) El-Gamal, M. I.; Al-Ameen, S. K.; Al-Koumi, D. M.; Hamad, M. G.; Jalal, N. A.; Oh, C.-H. Recent advances of colony-stimulating factor-1 receptor (CSF-1R) kinase and its inhibitors. *J. Med. Chem.* **2018**, *61*, 5450−5466.

(13) Tap, W. D.; Wainberg, Z. A.; Anthony, S. P.; Ibrahim, P. N.; Zhang, C.; Healey, J. H.; Chmielowski, B.; Staddon, A. P.; Cohn, A. L.; Shapiro, G. I.; Keedy, V. L.; Singh, A. S.; Puzanov, I.; Kwak, E. L.; Wagner, A. J.; Von Hoff, D. D.; Weiss, G. J.; Ramanathan, R. K.; Zhang, J.; Habets, G.; Zhang, Y.; Burton, E. A.; Visor, G.; Sanftner, L.; Severson, P.; Nguyen, H.; Kim, M. J.; Marimuthu, A.; Tsang, G.; Shellooe, R.; Gee, C.; West, B. L.; Hirth, P.; Nolop, K.; van de Rijn, M.; Hsu, H. H.; Peterfy, C.; Lin, P. S.; Tong-Starksen, S.; Bollag, G. Structure-guided blockade of CSF1R kinase in tenosynovial giant-cell tumor. *N. Engl. J. Med.* **2015**, *373*, 428−437.

(14) Pyonteck, S. M.; Akkari, L.; Schuhmacher, A. J.; Bowman, R. L.; Sevenich, L.; Quail, D. F.; Olson, O. C.; Quick, M. L.; Huse, J. T.; Teijeiro, V.; Setty, M.; Leslie, C. S.; Oei, Y.; Pedraza, A.; Zhang, J.; Brennan, C. W.; Sutton, J. C.; Holland, E. C.; Daniel, D.; Joyce, J. A. CSF-1R inhibition alters macrophage polarization and blocks glioma progression. *Nat. Med.* **2013**, *19*, 1264−1272.

(15) Bendell, J. C.; Tolcher, A. W.; Jones, S. F.; Beeram, M.; Infante, J. R.; Larsen, P.; Rasor, K.; Garrus, J. E.; Li, J. F.; Cable, P. L.; Eberhardt, C.; Schreiber, J.; Rush, S.; Wood, K. W.; Barret, E.; Patnaik, A. A phase 1 study of ARRY-382, an oral inhibitor of colony-stimulating factor-1 receptor (CSF1R), in patients with advanced or metastatic cancers. *Mol. Cancer Ther.* **2013**, *12*, A252.

(16) Von Tresckow, B.; Morschhauser, F.; Ribrag, V.; Topp, M. S.; Chien, C.; Seetharam, S.; Aquino, R.; Kotoulek, S.; de Boer, C. J.; Engert, A. An open-label, multicenter, phase I/II study of JNJ-40346527, a CSF-1R inhibitor, in patients with relapsed or refractory hodgkin lymphoma. *Clin. Cancer Res.* **2015**, *21*, 1843−1850.

(17) Mok, S.; Duffy, C.; Du, R.; Allison, J. P. Blocking colony stimulating factor 1 receptor (CSF-1R) and tropomyosin receptor kinase (Trk) improves antitumor efficacy of immunotherapy. *Cancer Immunol. Res.* **2017**, *5*, PR01.

https://dx.doi.org/10.1021/acs.jmedchem.9b01912
J. Med. Chem. XXXX, XXX, XXX−XXX

(18) Osipov, A.; Saung, M. T.; Zheng, L.; Murphy, A. G. Small molecule immunomodulation: the tumor microenvironment and overcoming immune escape. *J. Immunother. Cancer* **2019**, *7*, 224.
(19) Galanis, A.; Levis, M. Inhibition of c-Kit by tyrosine kinase inhibitors. *Haematologica* **2015**, *100*, e77−e79.
(20) Liu, Y.; Peng, X.; Guan, X.; Lu, D.; Xi, Y.; Jin, S.; Chen, H.; Zeng, L.; Ai, J.; Geng, M.; Hu, Y. Discovery of novel ponatinib analogues for reducing KDR activity as potent FGFRs inhibitors. *Eur. J. Med. Chem.* **2017**, *126*, 122−132.
(21) Zhao, Z.; Wu, H.; Wang, L.; Liu, Y.; Knapp, S.; Liu, Q.; Gray, N. S. Exploration of type II binding mode: a privileged approach for kinase inhibitor focused drug discovery? *ACS Chem. Biol.* **2014**, *9*, 1230−1241.
(22) Blanqué, R.; Meakin, C.; Millet, S.; Gardner, C. R. Selective enhancement of LPS-induced serum TNF-alpha production by carrageenan pretreatment in mice. *Gen. Pharmacol.* **1998**, *31*, 301−306.
(23) Trott, O.; Olson, A. J. AutoDock Vina: improving the speed and accuracy of docking with a new scoring function, efficient optimization, and multithreading. *J. Comput. Chem.* **2010**, *31*, 455−461.

https://dx.doi.org/10.1021/acs.jmedchem.9b01912
J. Med. Chem. XXXX, XXX, XXX−XXX